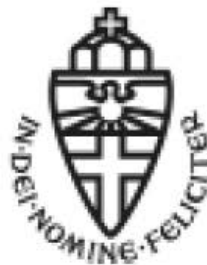


Radboud Universiteit



GRAPHENE FLAGSHIP



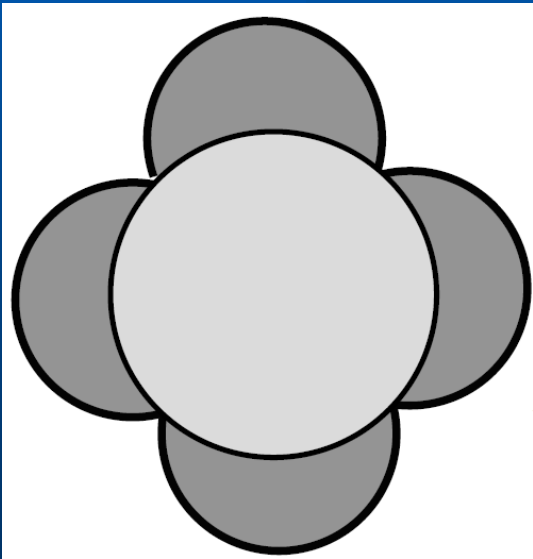
Semiclassical theory for massless Dirac fermions (and a bit of topology)

Mikhail Katsnelson

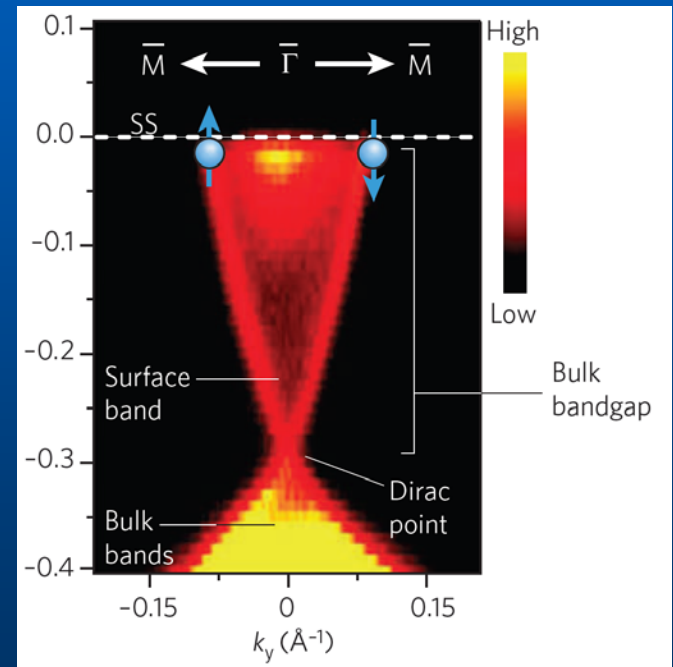
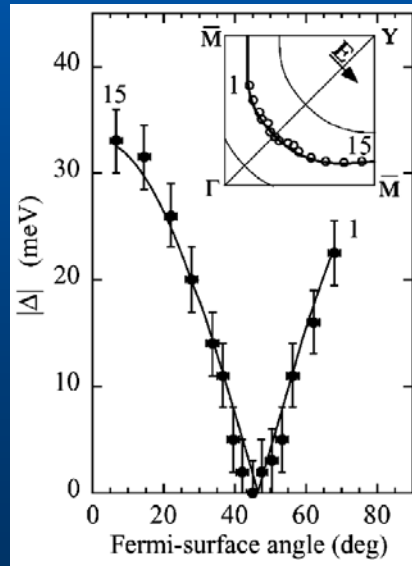
In collaboration with Koen Reijnders,
Timur Tudorovskiy, Sergey Dobrokhotov,
Dima Minenkov, and Vladimir Nazaikinskii

Massless Dirac fermions in condensed matter physics

1. d-wave superconductors
2. Vortices in superconductors and in superfluid helium-3
3. Topological insulators
4. Graphene

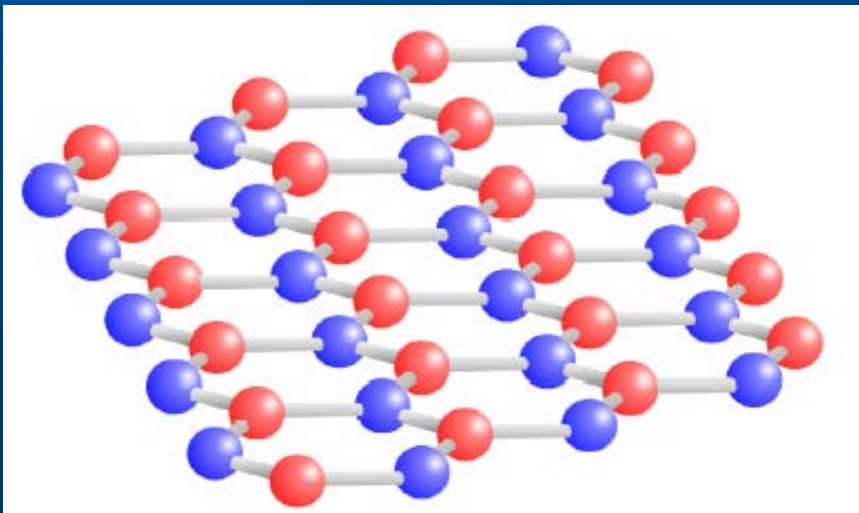
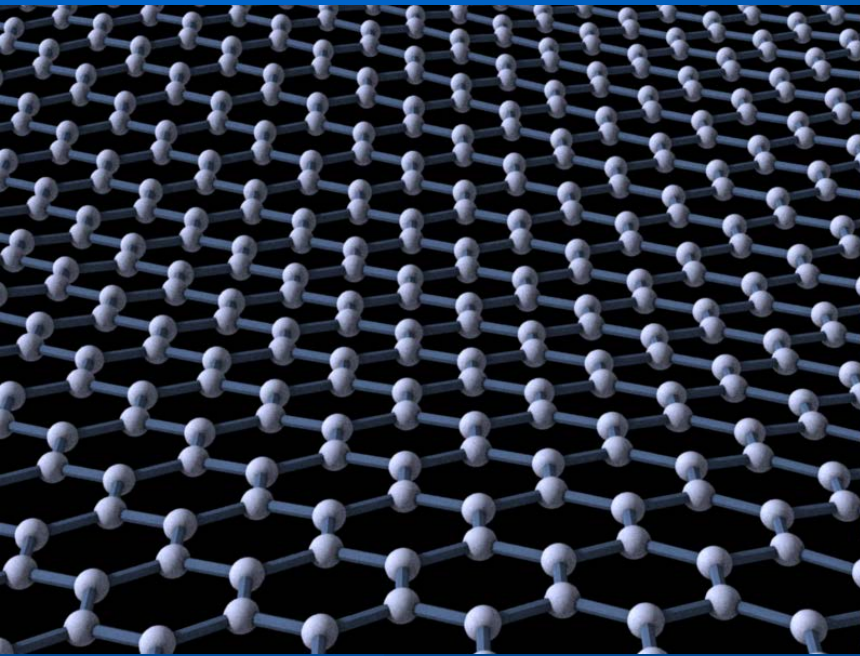


Gap in high-Tc cuprates



Electronic structure on surface of Bi_2Se_3

Honeycomb lattice (graphene)



Two equivalent sublattices,
A and B (pseudospin)

Massless Dirac fermions in graphene

$$H = -i\hbar c^* \begin{pmatrix} 0 & \frac{\partial}{\partial x} - i \frac{\partial}{\partial y} \\ \frac{\partial}{\partial x} + i \frac{\partial}{\partial y} & 0 \end{pmatrix} \quad \hbar c^* = \frac{\sqrt{3}}{2} \gamma_0 a$$

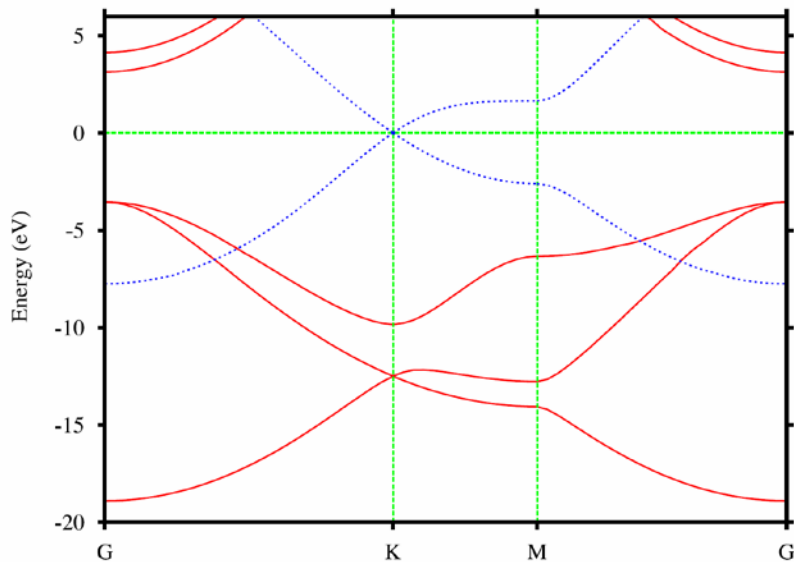
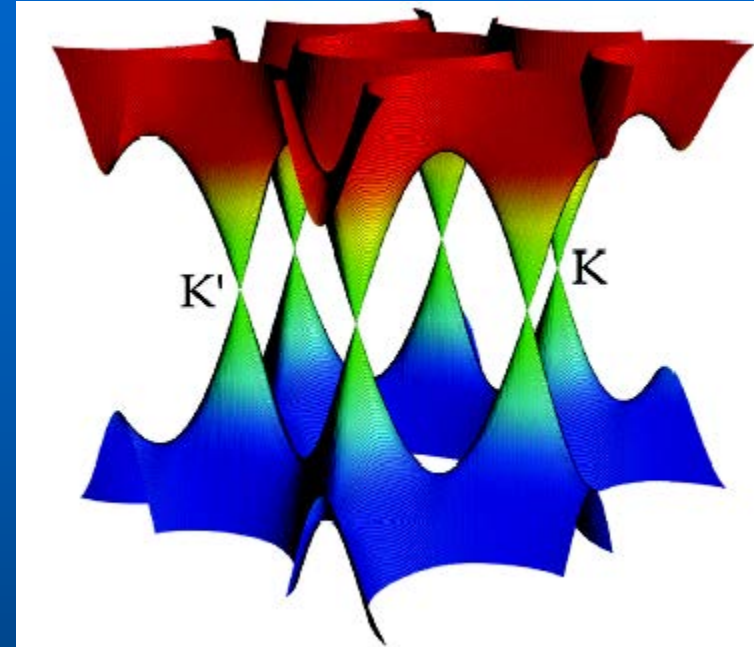


FIG. 2: (color online) Band structure of a single graphene layer. Solid red lines are σ bands and dotted blue lines are π bands.



sp^2 hybridization, π bands crossing the neutrality point

Neglecting intervalley scattering: massless Dirac fermions

Symmetry protected (T and I)

Outline

1. Chiral tunneling

Tudorovskiy, Reijnders, MIK, Phys. Scr. T 146, 014010 (2012);
Reijnders, Tudorovskiy, MIK, Ann. Phys. (NY) (2013)

2. Zero-mass lines

Tudorovskiy, MIK, Phys. Rev. B 86, 045419 (2012)

3. Aharonov-Bohm effect and spectral flow for massless Dirac fermions

MIK, Nazaikinskii, Theor. Math. Phys. 172, 1263 (2012)
Tudorovskiy, Nazaikinskii, MIK, Phys. Stat. Sol. RRL 7, 157 (2013)

Outline II

4. Electron Veselago lenses and caustics

Reijnders, MIK, Phys. Rev. B 95, 115310 (2017);

Reijnders, MIK, Phys. Rev. B 96, 045305 (2017);

5. Electron optics in 2D case

Reijnders, Minenkov, MIK, Dobrokhotov, Ann. Phys.(NY) 397, 65 (2018)

Koen Reijnders thesis (Nijmegen, 2019)

See also

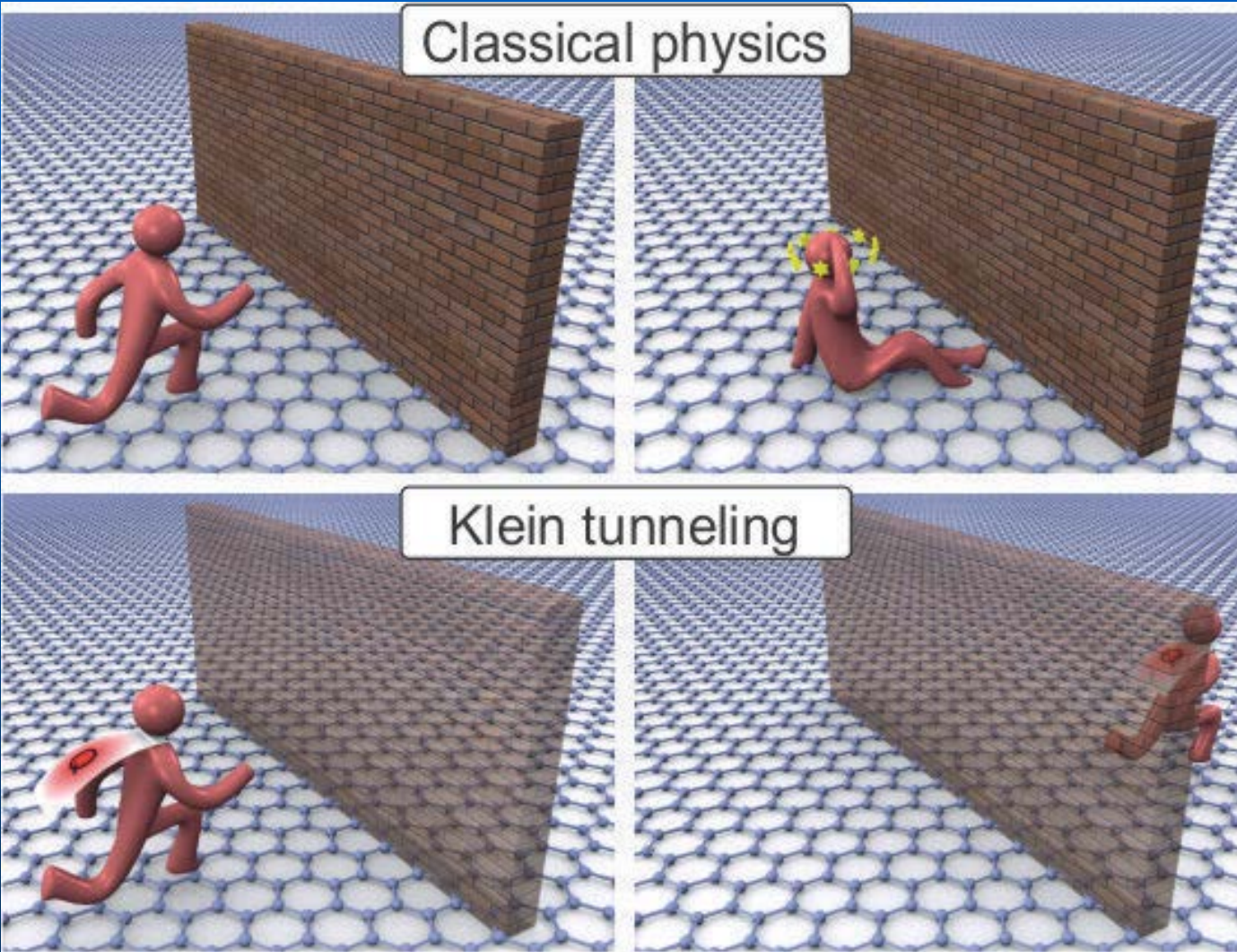
Semiclassical dynamics of charge carriers in graphene

<https://repository.ubn.ru.nl/handle/2066/204183>

Chiral tunneling and Klein paradox

MIK, Novoselov, Geim, Nat. Phys. 2, 620 (2006)

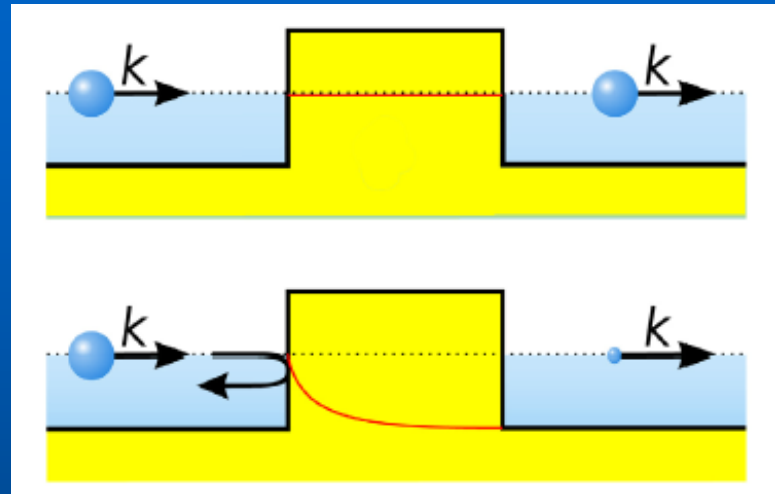
Electronics: heterostructures (p - n - p junctions etc.)



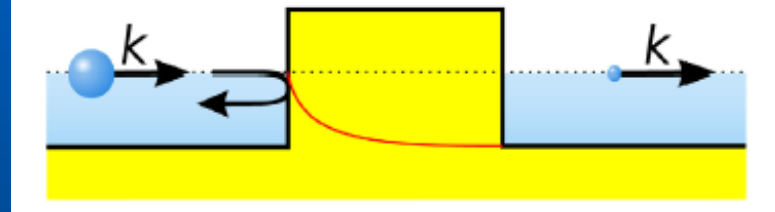
(C) Florian Sterl

Klein paradox II

Ultrarelativistic



Nonrelativistic



Tunnel effect: momentum and coordinate are complementary variables, kinetic and potential energy are not measurable simultaneously

Relativistic case: even the *coordinate itself* is not measurable, particle-antiparticle pair creation

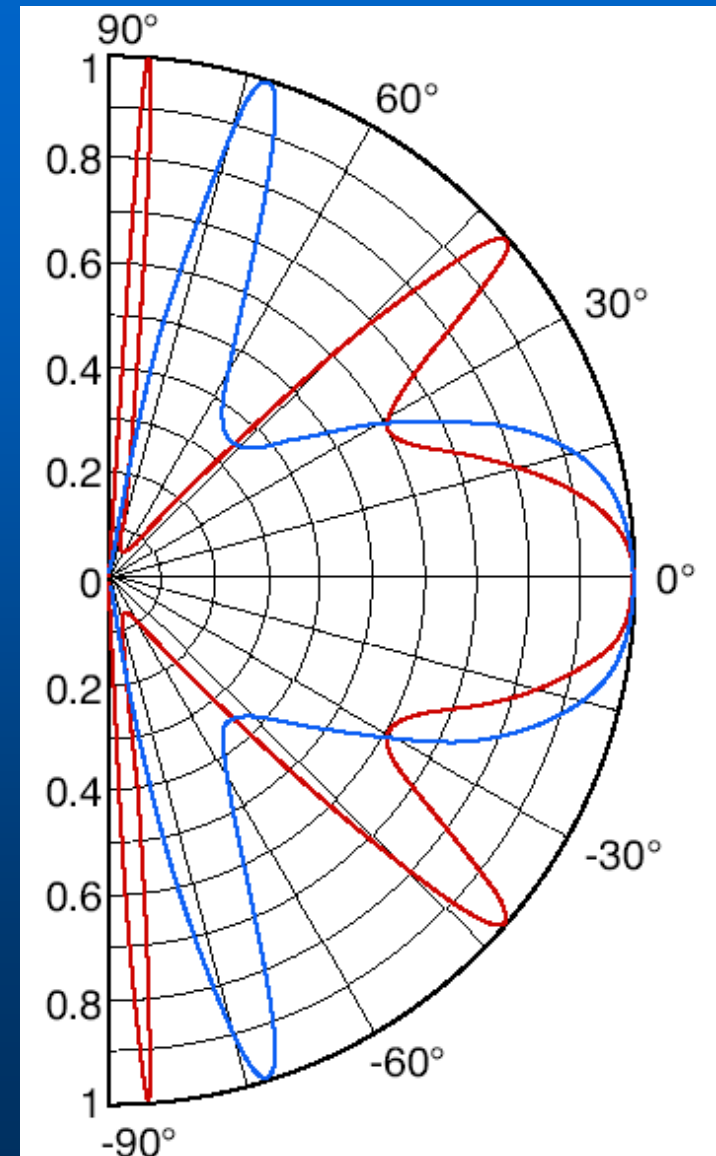
Klein paradox III

Transmission probability

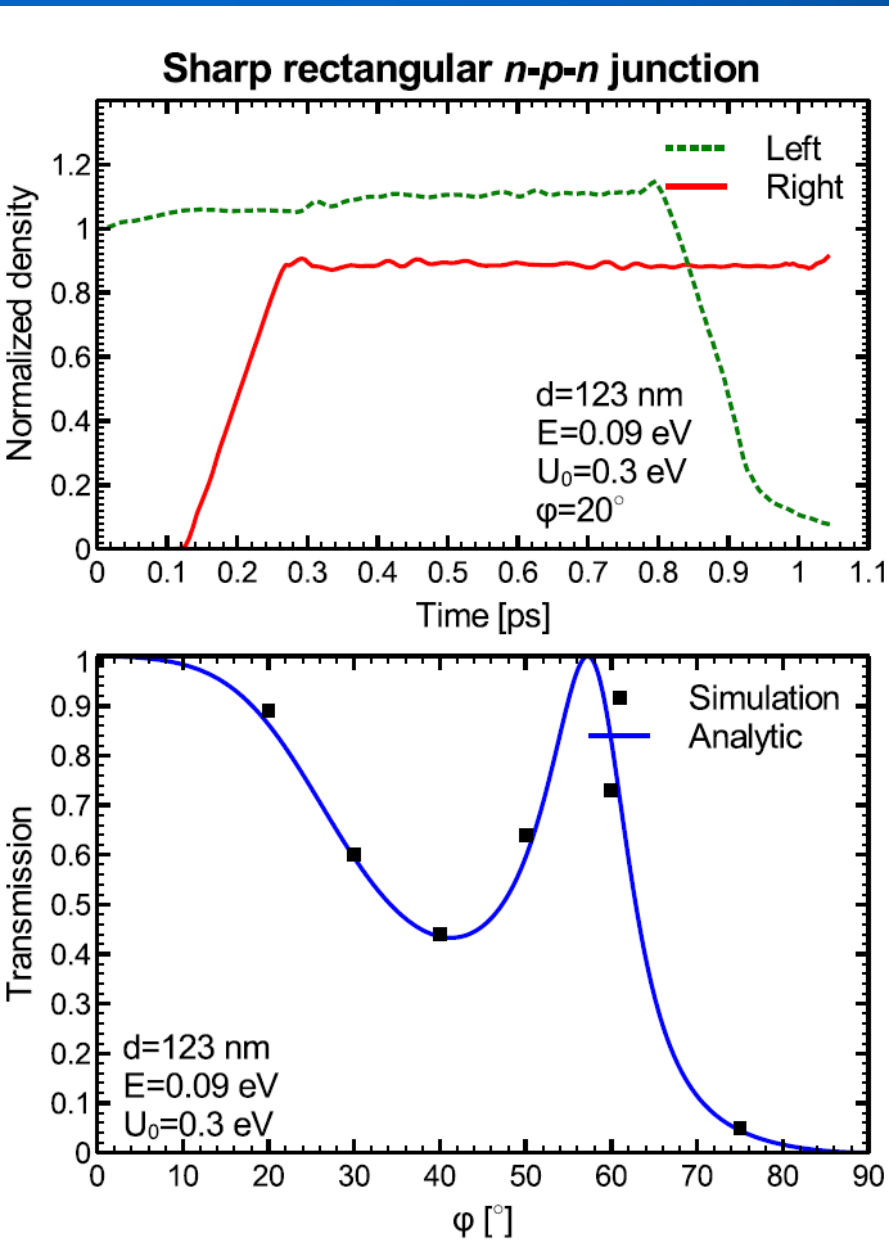
Barrier width 100 nm

Electron concentration
outside barrier $0.5 \times 10^{12} \text{ cm}^{-2}$

Hole concentration
inside barrier $1 \times 10^{12} \text{ cm}^{-2}$ (red)
and $3 \times 10^{12} \text{ cm}^{-2}$ (blue)



Klein paradox IV



Real-time simulations (numerical solution of time-dependent Schrödinger equation)

PHYSICAL REVIEW B **91**, 045420 (2015)

Modeling Klein tunneling and caustics of electron waves in graphene

R. Logemann, K. J. A. Reijnders, T. Tudorovskiy, M. I. Katsnelson, and Shengjun Yuan*

FIG. 4. (Color online) Transmission for a sharp rectangular n - p - n junction with $U_0 = 0.3$ eV, $E = 0.09$ eV, and $d = 123$ nm. (Top) Normalized densities in the “left” (green dashed line) and “right” (solid red line) measurement regions (see Fig. 1) as a function of time, from which the transmission for the incidence angle $\varphi = 20^\circ$ is extracted. (Bottom) Transmission as a function of incidence angle φ . The numerical results agree very well with the analytic solution (15).

Klein tunneling: Experimental confirmation

PRL **102**, 026807 (2009)

PHYSICAL REVIEW LETTERS

week ending
16 JANUARY 2009

Evidence for Klein Tunneling in Graphene p - n Junctions

N. Stander, B. Huard, and D. Goldhaber-Gordon*

Department of Physics, Stanford University, Stanford, California 94305, USA

(Received 13 June 2008; published 16 January 2009)

Transport through potential barriers in graphene is investigated using a set of metallic gates capacitively coupled to graphene to modulate the potential landscape. When a gate-induced potential step is steep enough, disorder becomes less important and the resistance across the step is in quantitative agreement with predictions of Klein tunneling of Dirac fermions up to a small correction. We also perform magnetoresistance measurements at low magnetic fields and compare them to recent predictions.

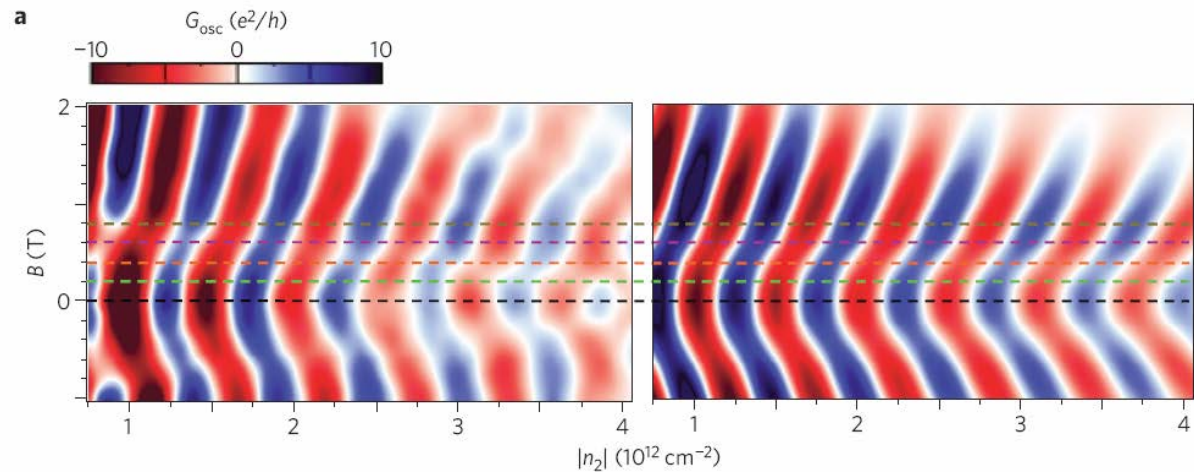
nature
physics

LETTERS

PUBLISHED ONLINE: 1 FEBRUARY 2009 | DOI: 10.1038/NPHYS1198

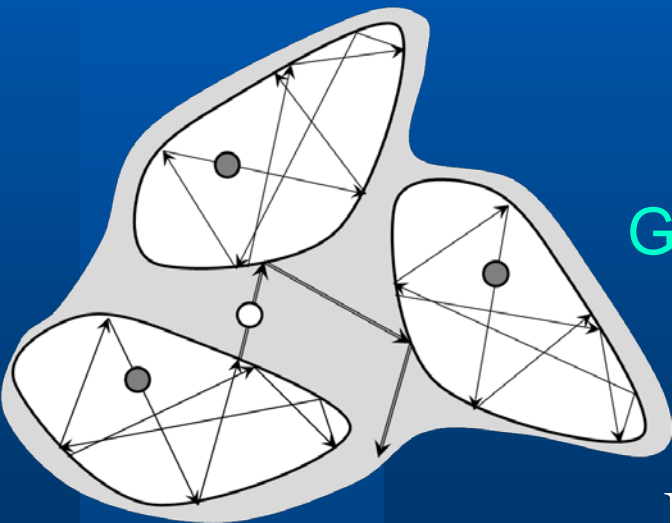
Quantum interference and Klein tunnelling in graphene heterojunctions

Andrea F. Young and Philip Kim*

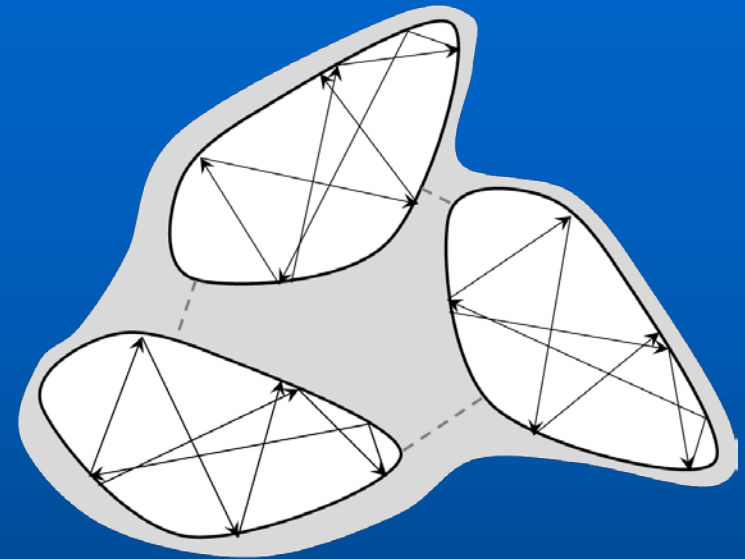


Klein tunneling prevents localization

Back scattering is
forbidden for chiral
fermions! Magic angle = 0
Nonuniversal magic angle
for bilayer exists!



Graphene



Conventional semiconductors

Electrons cannot be locked by random potential relief neither for single-layer nor for bilayer graphene – absence of localization and minimal conductivity?!

Ripples and puddles

Graphene on SiO₂

Gibertini, Tomadin, Guinea, MIK & Polini, Phys. Rev. B 85, 201405(R)(2012); Experimental STM data: V.Geringer et al (M.Morgenstern group)

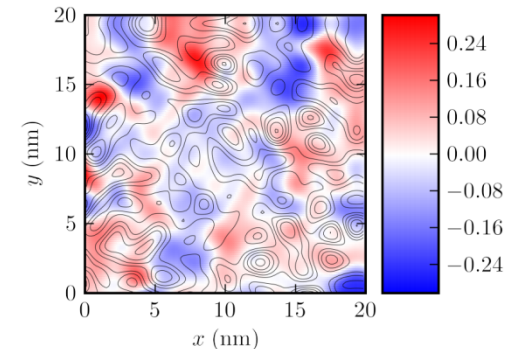
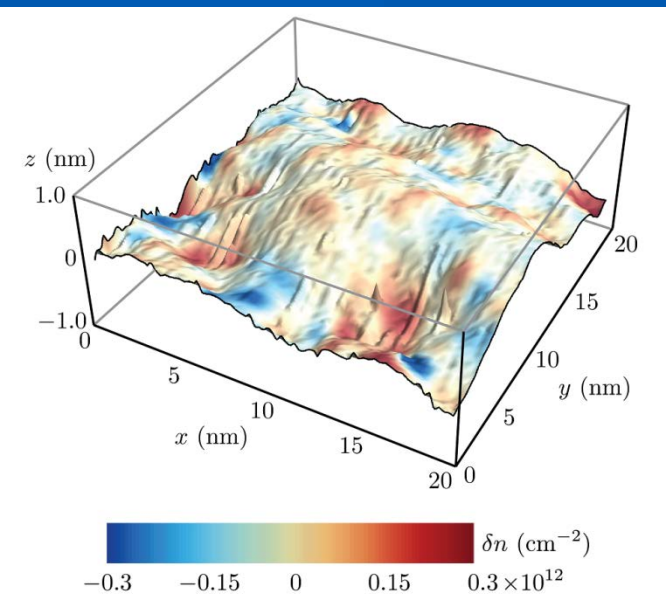


FIG. 3: (Color online) Fully self-consistent induced carrier-density profile $\delta n(\mathbf{r})$ (in units of 10^{12} cm^{-2}) in the corrugated graphene sheet shown in Fig. 1. The data reported in this figure have been obtained by setting $g_1 = 3 \text{ eV}$, $\alpha_{ee} = 0.9$, and an average carrier density $\bar{n}_c \approx 2.5 \times 10^{11} \text{ cm}^{-2}$. The thin solid lines are contour plots of the curvature $\nabla_{\mathbf{r}}^2 h(\mathbf{r})$. Note that there is no simple correspondence between topographic out-of-plane corrugations and carrier-density inhomogeneity.

Ripples are unavoidable; ripples induce puddles; without Klein tunneling graphene would be almost useless for electronic applications

One-dimensional barrier

T. Tudorovskiy, K. Reijnders & MIK, 2012, 2013

One-dimensional potential

$$\left[v \begin{pmatrix} 0 & \hat{p}_x - ip_y \\ \hat{p}_x + ip_y & 0 \end{pmatrix} + u(x/l) - E \right] \Psi = 0$$

$$\tilde{x} = x/l, \tilde{p}_x = -i\hbar d/d\tilde{x}, \tilde{p}_y = p_y/p_0, \hbar = \hbar/p_0 l, \tilde{u} = u/vp_0$$

$$\tilde{E} = E/vp_0$$

Skipping tildes: the Hamiltonian

$$\hat{H} = \begin{pmatrix} 0 & \hat{p}_x - ip_y \\ \hat{p}_x + ip_y & 0 \end{pmatrix} + u(x)$$

One-dimensional barrier II

Reduction to exact Schrödinger equations for complex potential

$$(\hat{p}_x^2 + p_y^2 - v(x)^2 - i\hbar\sigma_x v'(x))\Psi = 0$$

$$v(x) = u(x) - E$$

$$\Psi = \begin{pmatrix} 1 \\ 1 \end{pmatrix} \eta_1 + \begin{pmatrix} 1 \\ -1 \end{pmatrix} \eta_2$$

$$\left(\hbar^2 \frac{d^2}{dx^2} + v(x)^2 - p_y^2 \pm i\hbar v'(x) \right) \eta_{1,2} = 0$$

Schrödinger equation with complex potential

Classical equations

Classical dynamics is described by the Hamiltonian

$$L_0^\pm(\mathbf{p}_x, \mathbf{x}) = \pm|\mathbf{p}| + u(\mathbf{x}) \text{ for electrons and holes}$$

Turning points $u(x_0) = E$

Electron and hole Hamiltonians coincide for normal incidence:

$$p_x = p_y = 0$$

Squared Hamiltonian equations: $\mathcal{L}(\mathbf{p}_x, \mathbf{x}) \equiv p_x^2 - v^2(\mathbf{x}) = -p_y^2$

$$\epsilon = -p_y^2 \text{ plays the role of energy}$$

Classical phase portrait

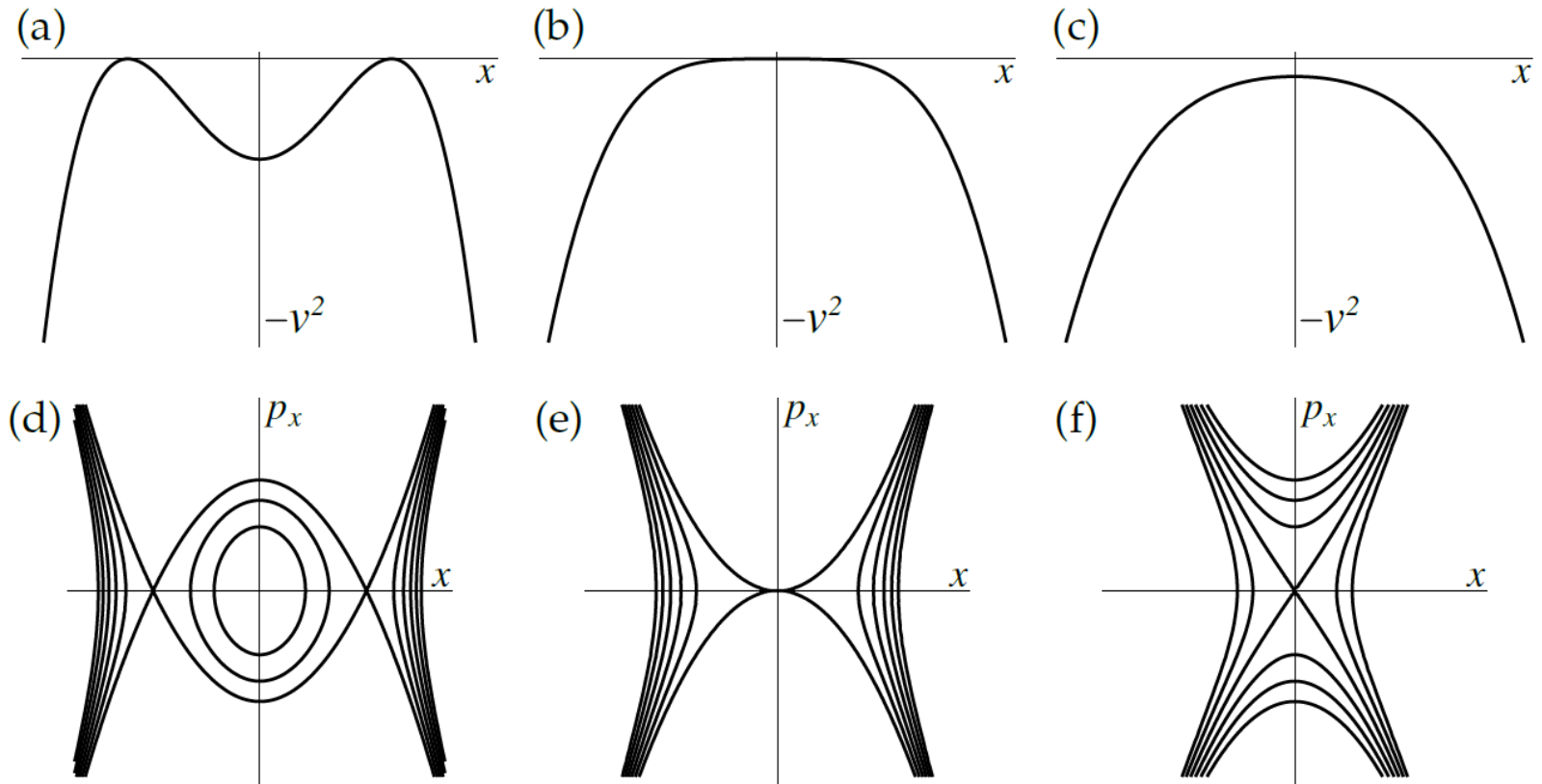


Figure 2.2: (a)–(c): Effective potential $-v^2(x)$ for the potential $u(x) = -x^2$ when (a) $E < 0$, (b) $E = 0$, (c) $E > 0$. (d)–(f): Phase portraits of the Hamiltonian systems that originate from \mathcal{L} , for the energies (d) $E < 0$, (e) $E = 0$, (f) $E > 0$. The different lines in each phase portrait correspond to different values of p_y .

Semiclassical theory

Exact equations (continued to the complex plane $x \rightarrow z$)

$$\left(\hbar^2 \frac{d^2}{dz^2} + v^2(z) - p_y^2 + i\hbar v'(z) \right) \eta_1(z) = 0$$

$$\eta_2 = \frac{1}{p_y} \left(\hbar \frac{d}{dz} + iv(z) \right) \eta_1(z)$$

Semiclassical solution

$$\eta_1(z) = A(z, \hbar) e^{is(z)/\hbar}$$

$$A(z, \hbar) = A_0(z) + \hbar A_1(z) + \dots$$

Semiclassical theory II

Exact:

$$\left[\left(\hbar \frac{d}{dz} + i s'(z) \right)^2 + v^2(z) - p_y^2 + i \hbar v'(z) \right] A(z, \hbar) = 0$$

Zeroth order in \hbar $(s'(z))^2 = v^2(z) - p_y^2$

First order in \hbar $2s'(z)A_0'(z) + s''(z)A_0(z) + v'(z)A_0(z) = 0$

$$\frac{d}{dz} [s'(z)A_0^2(z)] + v'(z)A_0^2(z) = 0$$

Semiclassical theory III

Solution:

$$A_0^2(z) = \frac{B}{s'(z)} \exp \left(- \int_{z_0}^z d\zeta \frac{v'(\zeta)}{s'(\zeta)} \right)$$

$$\tilde{\eta}_1^\pm(z) = \frac{1}{p_x^{1/2}(z)} \exp \left(\mp \frac{1}{2} \int_{z_0}^z d\zeta \frac{v'(\zeta)}{p_x(\zeta)} \right) \exp \left(\pm \frac{i}{\hbar} s(z_0, z) \right)$$

$$s(z_0, z) = \int_{z_0}^z p_x(\zeta) d\zeta, \quad \text{with } p_x(z) = \left(v^2(z) - p_y^2 \right)^{1/2}$$

The integral is calculated explicitly

$$\int_{z_0}^z d\zeta \frac{v'(\zeta)}{p_x(\zeta)} = \int_{v(z_0)}^{v(z)} \frac{dv}{(v^2 - p_y^2)^{1/2}} = \ln \left[\frac{v(z) + (v^2(z) - p_y^2)^{1/2}}{|p_y|} \right] + \text{const}$$

Semiclassical theory IV

Fundamental semiclassical solutions

$$\eta_1(x) = \frac{a_1}{\sqrt{p_x(x)}\sqrt{G(x)}} e^{iS(x_0,x)/\hbar} + a_2 \frac{\sqrt{G(x)}}{\sqrt{p_x(x)}} e^{-iS(x_0,x)/\hbar}$$

$$\eta_2(x) = i\alpha_v \frac{|p_y|}{p_y} \left(a_1 \frac{\sqrt{G(x)}}{\sqrt{p_x(x)}} e^{iS(x_0,x)/\hbar} + a_2 \frac{1}{\sqrt{p_x(x)}\sqrt{G(x)}} e^{-iS(x_0,x)/\hbar} \right)$$

$$G(x) = \left(\frac{|v(x)| + p_x(x)}{|p_y|} \right)^{\alpha_v}, \quad \alpha_v = \text{sgn}[v(x_0)]$$

$$p_x(x) = \sqrt{v^2(x) - p_y^2}, \quad S(x_0, x) = \int_{x_0}^x p_x(\zeta) d\zeta$$

Stokes diagrams

The semiclassical solutions are divergent at the turning points

$$p_x(z_0) = 0$$

The matching of solutions in various regions can be done in complex plane when we can go around the turning point at some safe distance

General complex WKB:
$$h^2 \frac{d^2 \psi}{dz^2} + q(z) \psi(z) = 0 \quad h \ll 1$$

Fundamental semiclassical solutions

$$f_1(z_0, z) = q^{-1/4} \exp \left(\frac{i}{h} \int_{z_0}^z dz' q^{1/2}(z') \right),$$
$$f_2(z_0, z) = q^{-1/4} \exp \left(-\frac{i}{h} \int_{z_0}^z dz' q^{1/2}(z') \right)$$

Stokes diagrams II

$$s(z_0, z) = \int_{z_0}^z q^{1/2}(z') dz'$$

Anti-Stokes lines: the function s is real. Both fundamental solutions are comparable in their amplitude at these lines.

(Stokes lines: the function s is imaginary – less important)

At each anti-Stokes lines

$$\psi(z) = C_1^\gamma f_1(z_0, z) + C_2^\gamma f_2(z_0, z)$$

Stokes phenomenon: there are jumps in the coefficients (and they are roughly associated to Stokes lines)

So, the exact solution has different representations in different sectors of the complex plane

Stokes diagrams III

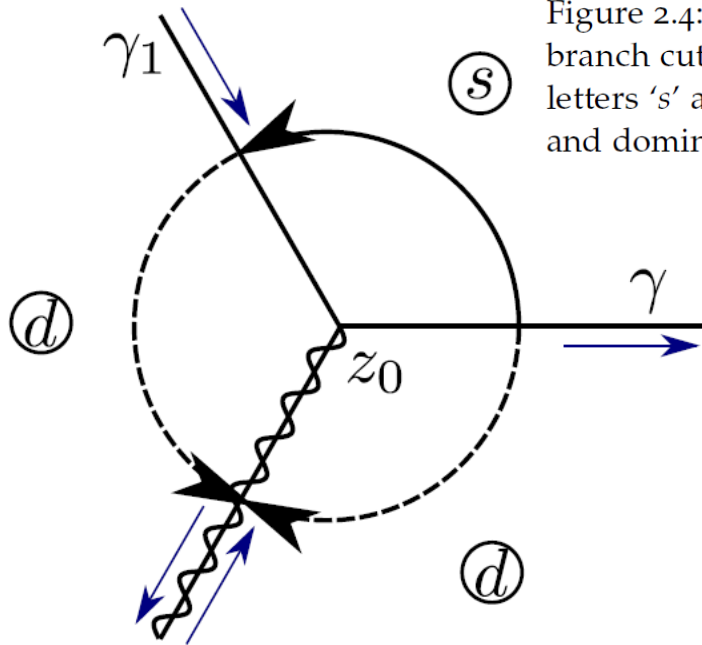


Figure 2.4: The Stokes diagram for a simple turning point z_0 . The wavy line depicts the branch cut. The blue arrows show the direction of the growth of the action $s(z_0, z)$. The letters 's' and 'd' indicate the sectors where the asymptotic solution η_1^+ is subdominant and dominant, respectively.

$$\begin{pmatrix} C_1^{\gamma_1} \\ C_2^{\gamma_1} \end{pmatrix} = M \begin{pmatrix} C_1^\gamma \\ C_2^\gamma \end{pmatrix}$$

M is the connection matrix

The coefficients of subdominant terms can be changed at the background of exponentially large dominant terms

Different methods to find connection matrix and thus to build semiclassical equations available in almost the whole complex plane (Zwaan method, the method of comparison equations...)

Stokes diagrams IV

Scattering problem: connecting propagating (not evanescent!) waves in different regions, that is, transition from one anti-Stokes line to the other anti-Stokes line, that is, calculation of connection matrix

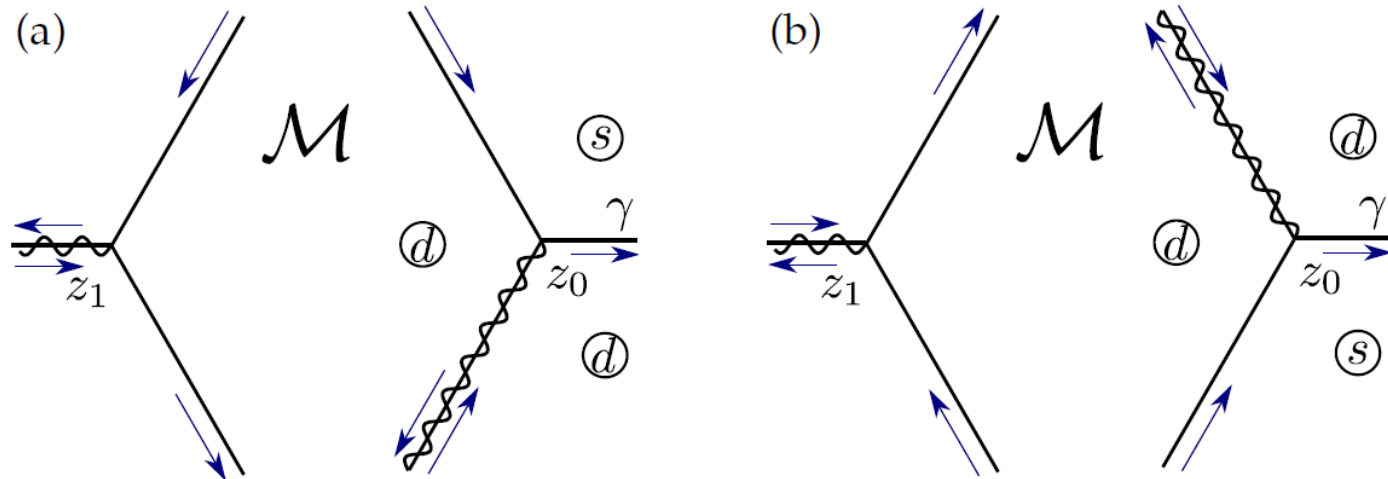
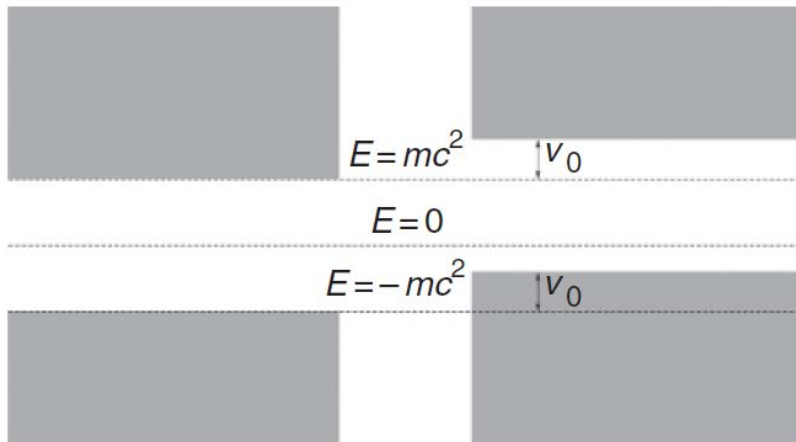


Figure 2.5: The Stokes diagram for two simple turning points z_0 and z_1 . The blue arrows show the direction in which the action $s(z_0, z)$ increases and the wavy lines depict the branch cuts. The division of the different sectors in dominant or subdominant is performed with respect to z_0 . In diagram (a), we consider $\eta_1(z) = \eta_1^+(z)$ along γ and in diagram (b) we consider $\eta_1(z) = \eta_1^-(z)$ along γ .

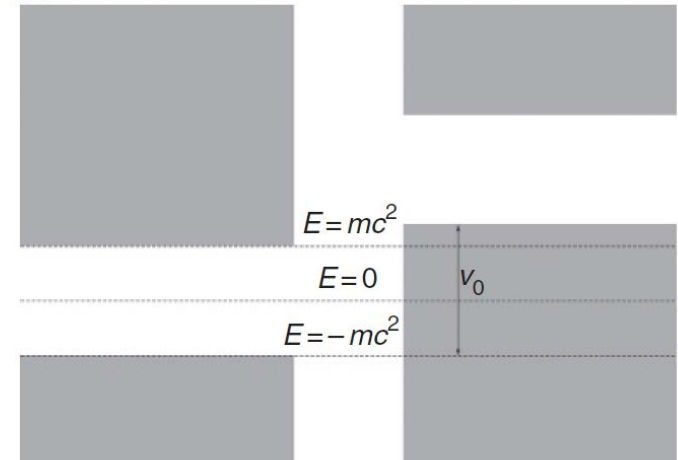
Different cases

1. $E < u_0$, $|p_y| < u_0 - E$: Klein tunneling regime, or tunneling through a barrier supporting hole states
2. $E > u_0$, $|p_y| < E - u_0$: above-barrier scattering
3. $E < u_0$ and $|p_y| > u_0 - E$, or $E > u_0$, $|p_y| > E - u_0$: conventional tunneling regime, tunneling through a barrier without hole states.

(a)



(b)



Difference between conventional case and Klein tunneling for real Dirac particles

Different cases II

Classical mechanics:

$$E = \pm|p| + u(x)$$

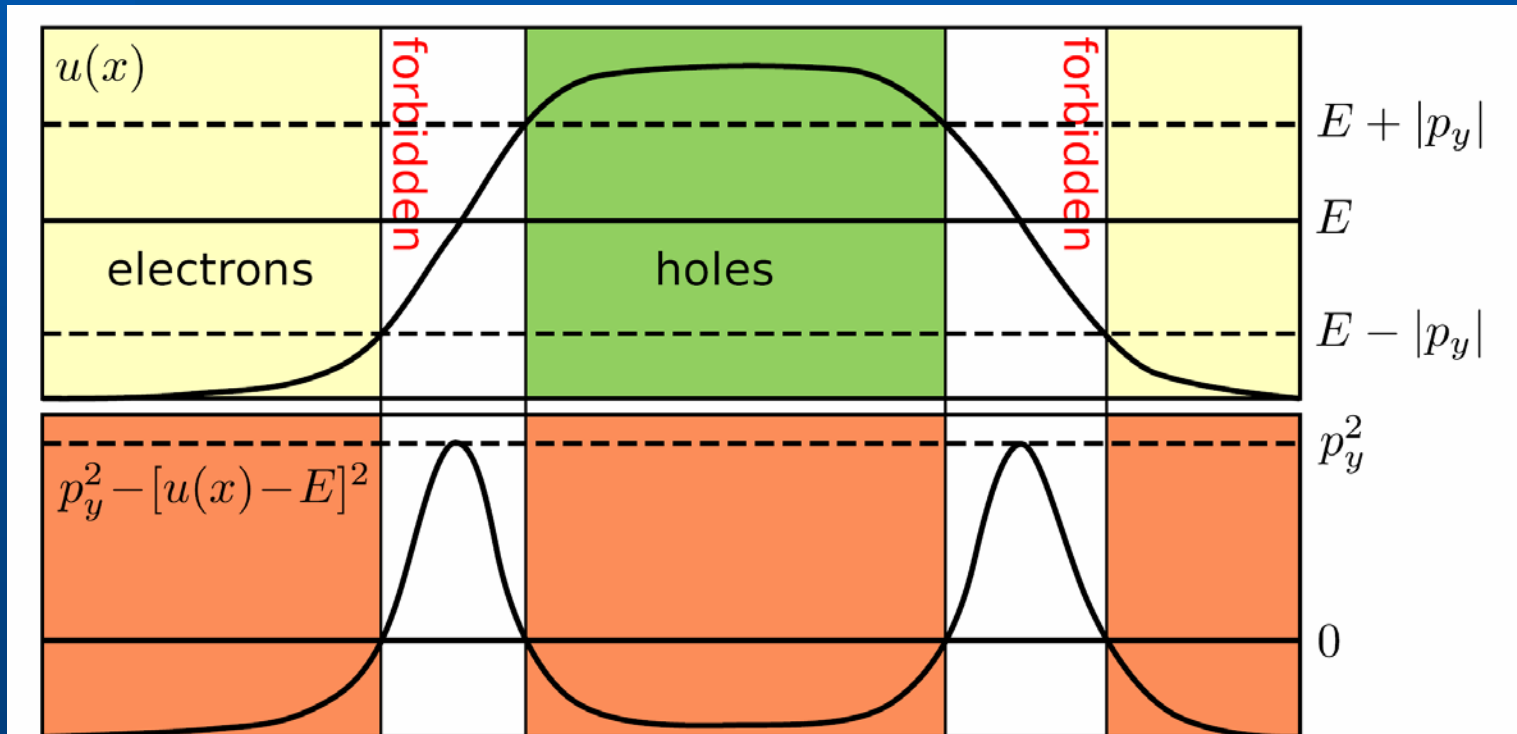
Effective Hamiltonian

$$\mathcal{L}(p_x, x) = p_x^2 - v^2(x) = -p_y^2$$

$$v(x) = u(x) - E$$

The case of Klein tunneling

$$E < U_{\max}, |p_y| < U_{\max} - E$$



Different cases III

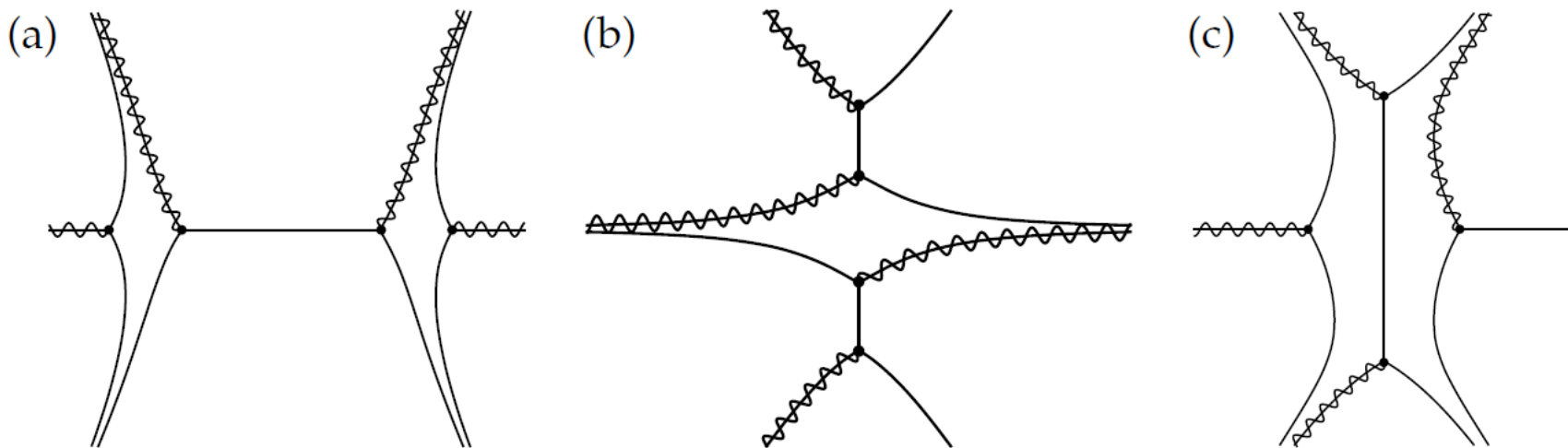


Figure 2.3: Stokes diagrams for the three different regimes outlined in section 2.2: (a) Klein tunneling, (b) above-barrier scattering and (c) conventional tunneling. Bold points show the turning points, the solid lines correspond to anti-Stokes lines and the wavy lines designate branch cuts of the function $(z - z_0)^{1/2}$. This figure was created using the potential $u(z) = -z^2$.

Klein tunneling – four real turning points; above-barrier scattering – four complex turning points

Method of comparison equations

$$h^2 \frac{d^2 \psi}{dz^2} + R(z, h) \psi(z) = 0$$

$$R(z, h) = \sum_{n=0}^{\infty} R_n(z) h^n$$

Map it to a related equation

$$h^2 \frac{d^2 V}{d\phi^2} + Q(\phi, h) V(\phi) = 0$$

which we can hope to solve (Q will be specified later)

$$\psi(z, h) = (\phi'(z))^{-1/2} V(\phi(z))$$

$\phi(z)$ is non-singular, i.e. ϕ' does not vanish

$$h^2 \left(\frac{3 (\phi'')^2}{4 (\phi')^2} - \frac{\phi'''}{2\phi'} \right) - Q(\phi, h) (\phi')^2 + R(z, h) = 0$$

Method of comparison equations II

$$Q(\phi, h) = \sum_{n=0}^{\infty} Q_n(\phi) h^n$$

and compare term by term:

$$\phi(z, h) = \sum_{n=0}^{\infty} \phi_n(z) h^n.$$

$$Q_0(\phi_0)(\phi'_0)^2 = R_0(z)$$

$Q_0(\phi_0)$ and $R_0(z)$ have the same number of turning points

$$Q_1(\phi_0)(\phi'_0)^2 + Q'_0(\phi_0)\phi_1(\phi'_0)^2 + 2Q_0(\phi_0)\phi'_0\phi'_1 = R_1(z)$$

$$\phi_1(z) = \frac{1}{2}\phi'_0 R_0^{-1/2} \int_{z_0}^z dz' R_0^{-1/2} (R_1 - (\phi'_0)^2 Q_1(\phi_0))$$

etc., term by term

Method of comparison equations III

Suppose R_0 has zeros (turning points) of the order m_j at $z = z_j$

Then, Q can be chosen as a polynomial:

$$Q_0(\phi) = \gamma_{\mu 0} \prod_{j=0}^N (\phi - \phi_0(z_j))^{m_j}$$

$$\int_{\phi_0(z_0)}^{\phi_0(z)} ds \prod_{j=0}^N [s - \phi_0(z_j)]^{m_j/2} = \int_{z_0}^z dz' [\gamma_{\mu 0}^{-1} R_0(z')]^{1/2}$$

Putting $z = z_j$ we find all constants $\phi_0(z_j)$ except one

Application to Dirac equation

$$R_0(x) = v^2(x) - p_y^2, \quad R_1(x) = iv'(x)$$

The single first-order turning point

$$\frac{2}{3} \Phi_0^{3/2}(x) = \int_{x_0}^x dx' R_0^{1/2}(x')$$

$$\phi_1(x) = \frac{1}{2} \phi_0' R_0^{-1/2} \int_{x_0}^x \frac{R_1(x')}{R_0^{1/2}(x')} dx'$$

Application to Dirac equation II

The comparison equation is Airy equation

$$h^2 \frac{d^2 V}{d\phi^2} + \phi V(\phi) = 0$$

$$V(\phi) = c_1 \text{Ai}(-h^{-2/3} \phi) + c_2 \text{Bi}(-h^{-2/3} \phi)$$

For small h we can use the asymptotics:

$$\xi \rightarrow \infty$$

$$\text{Ai}(\xi) = \frac{e^{-\frac{2}{3}\xi^{3/2}}}{2\sqrt{\pi}\xi^{1/4}},$$

$$\text{Bi}(\xi) = \frac{e^{\frac{2}{3}\xi^{3/2}}}{\sqrt{\pi}\xi^{1/4}},$$

$$\text{Ai}(-\xi) = \frac{\sin\left(\frac{2}{3}\xi^{3/2} + \frac{1}{4}\pi\right)}{\sqrt{\pi}\xi^{1/4}},$$

$$\text{Bi}(-\xi) = \frac{\cos\left(\frac{2}{3}\xi^{3/2} + \frac{1}{4}\pi\right)}{\sqrt{\pi}\xi^{1/4}}$$

Application to Dirac equation III

$$(\hbar^{-2/3} \phi)^{3/2} = \frac{1}{\hbar} \phi_0^{3/2} + \frac{3}{2} \phi_0^{1/2} \phi_1 + \mathcal{O}(\hbar)$$

$$\phi_0^{1/2} \phi_0' = R_0^{1/2}$$

Fundamental semiclassical solutions

$$\tilde{\eta}_1^\pm(x) = \frac{1}{R_0^{1/4}} \exp\left(\pm \frac{i}{2} \int_0^x \frac{R_1}{R_0^{1/2}} dx'\right) \exp\left(\pm \frac{i}{\hbar} \int_0^x R_0^{1/2} dx'\right)$$

They can be compared with asymptotics of Airy functions

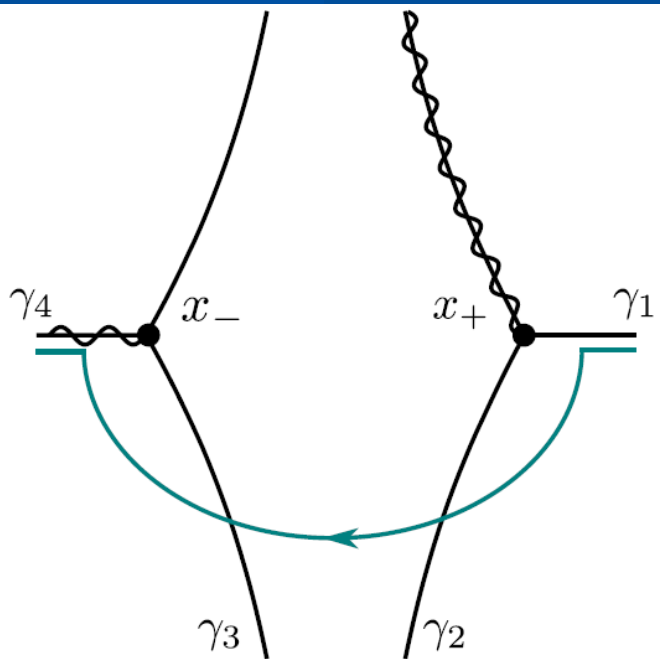
Application to Dirac equation IV

For left-propagating and right-propagating waves we find

$$c_{+,\infty} \tilde{\eta}_1^+ + c_{-,\infty} \tilde{\eta}_1^- \rightarrow (-ic_{+,\infty} + c_{-,\infty}) \tilde{\eta}_1^-$$

$$c_{+,\infty} = e^{i\pi/4} \pi^{-1/2} (-ic_1 + c_2)/2$$

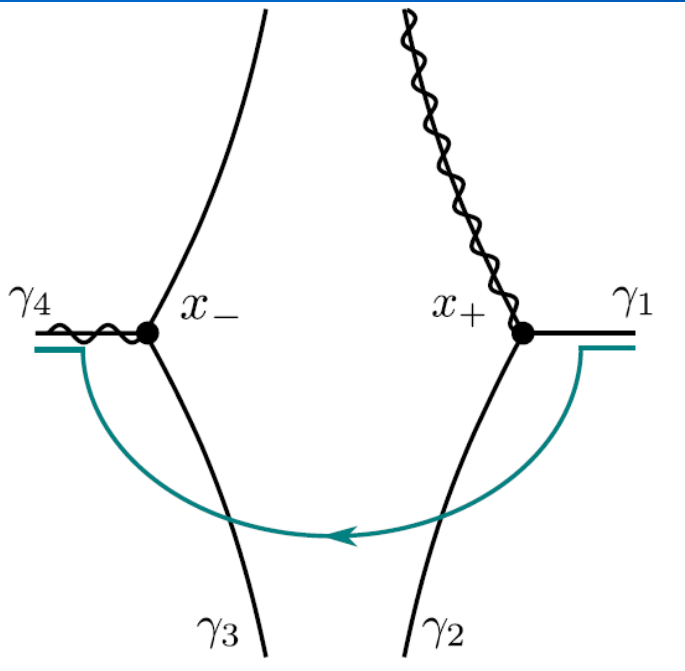
$$c_{-,\infty} = e^{-i\pi/4} \pi^{-1/2} (ic_1 + c_2)/2$$



So, for n-p junction if one considers two turning points separately one has:

$$\begin{pmatrix} C_1^{\gamma_2} \\ C_2^{\gamma_2} \end{pmatrix} = \begin{pmatrix} 1 & 0 \\ -i & 1 \end{pmatrix} \begin{pmatrix} C_1^{\gamma_1} \\ C_2^{\gamma_1} \end{pmatrix}$$

Application to Dirac equation V



$$\begin{pmatrix} C_1^{\gamma_4} \\ C_2^{\gamma_4} \end{pmatrix} = \begin{pmatrix} 1 & i \\ 0 & 1 \end{pmatrix} \begin{pmatrix} C_1^{\gamma_3} \\ C_1^{\gamma_3} \end{pmatrix}$$

At last, taking into account only dominant term between anti-Stokes lines:

$$\begin{pmatrix} C_1^{\gamma_3} \\ C_2^{\gamma_3} \end{pmatrix} = \begin{pmatrix} 0 & 0 \\ 0 & e^{-is(x_+, x_-)/\hbar} \end{pmatrix} \begin{pmatrix} C_1^{\gamma_2} \\ C_2^{\gamma_2} \end{pmatrix}$$

Application to Dirac equation VI

What happens if we take into account both turning points simultaneously?

$$x_- < x_+ \quad m_0 = m_1 = 1 \text{ and } \mu = 2 \quad \text{Put } \gamma_{20} = 1$$

$$\phi_0(x_-) = -\phi_0(x_+) = -a$$

Then we find

$$\frac{\pi a^2}{2} = \int_{x_-}^{x_+} \sqrt{p_y^2 - v^2(x)} dx = K$$

Similar, we find $\phi_1(x)$ and the comparison equation

$$h^2 \frac{d^2 V}{d\phi^2} + (\phi^2 - a^2 + ih) V(\phi) = 0$$

Application to Dirac equation VII

General solution in terms of parabolic cylinder functions:

$$V(\xi) = c_1 D_\nu(\sqrt{2}e^{i\pi/4}h^{-1/2}\phi) + c_2 D_{-\nu-1}(\sqrt{2}e^{3i\pi/4}h^{-1/2}\phi), \quad \nu = \frac{ia^2}{2h}$$

Asymptotics for small h

$$D_\nu(z) = \begin{cases} z^\nu e^{-z^2/4}, & -\pi/2 < \arg(z) \leq \pi/2 \\ z^\nu e^{-z^2/4} - z^{-\nu-1} e^{z^2/4} e^{-i\pi\nu} \frac{\sqrt{2\pi}}{\Gamma(-\nu)}, & \arg(z) \leq -\pi/2 \\ z^\nu e^{-z^2/4} - z^{-\nu-1} e^{z^2/4} e^{i\pi\nu} \frac{\sqrt{2\pi}}{\Gamma(-\nu)}, & \arg(z) > \pi/2, \end{cases}$$

Then,

$$\psi(x) = (\phi'(x))^{-1/2} V(\phi(x)) \text{ etc.}$$

Application to Dirac equation VIII

The expression for scattering matrix for n-p and p-n junctions:

$$T_{np} = \begin{pmatrix} e^{K/h} & \sqrt{e^{2K/h} - 1} e^{-i\theta - i\pi/2} \\ \sqrt{e^{2K/h} - 1} e^{i\theta - i\pi/2} & -e^{K/h} \end{pmatrix}$$

$$T_{pn} = \begin{pmatrix} e^{K/h} & \sqrt{e^{2K/h} - 1} e^{i\theta + i\pi/2} \\ \sqrt{e^{2K/h} - 1} e^{-i\theta + i\pi/2} & -e^{K/h} \end{pmatrix}$$

$$K = \int_{x_-}^{x_+} \sqrt{p_y^2 - v^2(x)} dx$$

$$\theta = \text{Arg} \left[\Gamma \left(1 + i \frac{K}{\pi h} \right) \right] - \frac{\pi}{4} + \frac{K}{\pi h} - \frac{K}{\pi h} \ln \left(\frac{K}{\pi h} \right)$$

p-n-p junction

Comparison equation with four turning points is too complicated, and no analytical solution is known, therefore we consider p-n and n-p junctions separately

Transmission probability

$$t_{npn} = \frac{e^{-K_{np}/\hbar} e^{-K_{pn}/\hbar} e^{-iL/\hbar}}{1 - \sqrt{1 - e^{-K_{np}/\hbar}} \sqrt{1 - e^{-K_{pn}/\hbar}} e^{-2iL/\hbar + i\pi - i\theta_{np} - i\theta_{pn}}}$$

$$K_{np} = \int_{x_1}^{x_2} dx \sqrt{p_y^2 - v^2(x)}$$

$x_{1,2}$ are turning points

$$v^2(x_0) - p_y^2 = 0$$

$$L = \int_{x_2}^{x_3} dx' \sqrt{v^2(x') - p_y^2}$$

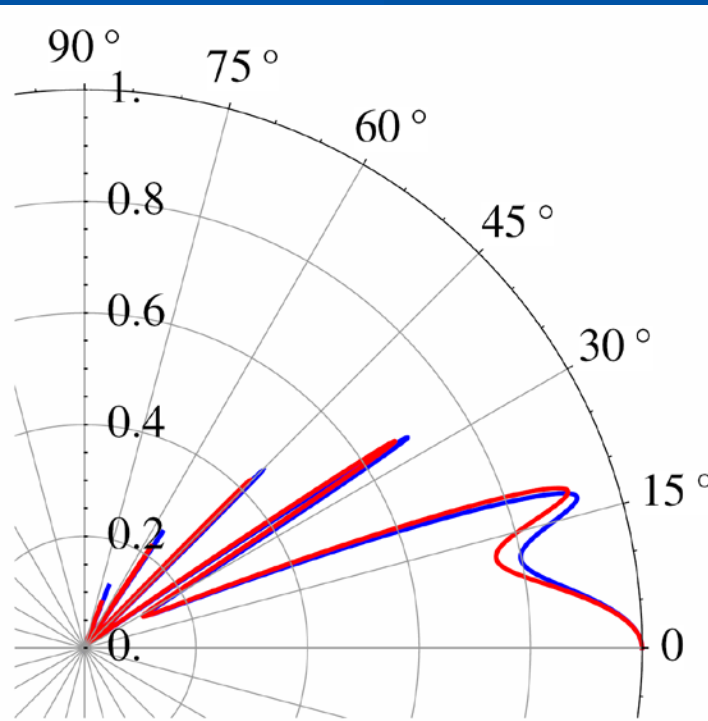
$$\theta = \text{Arg} \left[\Gamma \left(1 + i \frac{K}{\pi \hbar} \right) \right] - \frac{\pi}{4} + \frac{K}{\pi \hbar} - \frac{K}{\pi \hbar} \ln \left(\frac{K}{\pi \hbar} \right)$$

Fabri-Perot resonances

Magic angles with 100% transmission survives only for symmetric barriers (except normal incidence)

$$|t_{\text{res}}| = \frac{1}{\cosh(K_{np}/h - K_{pn}/h)}$$

$$K_{np}/h \gg 1, K_{pn} \gg 1$$



$$u(x/l_1) = \frac{u_{\text{max}}}{2} \left[1 + \tanh \left(10 \frac{x}{l_1} - 5 \right) \right]$$

The angular dependence of the transmission coefficient for a particle of energy 80 meV incident on an n-p-n junction of height 200 meV. The barrier width $l_2 = 250$ nm and the n-p and p-n regions have characteristic lengths $l_1 = 150$ nm and $l_3 = 50$ nm, respectively. The blue line shows the numerical results for 99 steps, while the red line shows the uniform approximation (5.77).

Very nice agreement with numerics

Comparison with numerics

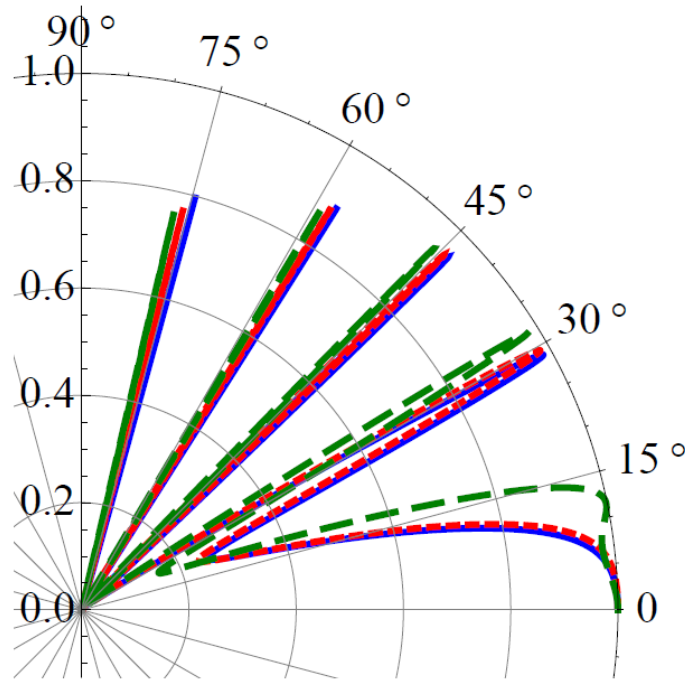


Figure 5: The angular dependence of the transmission coefficient for a particle of energy 100 meV incident on an n-p-n junction of height 250 meV. The barrier width $l_2 = 150$ nm and the n-p and p-n regions have characteristic lengths $l_1 = 70$ nm and $l_3 = 90$ nm, respectively. The blue (solid) line shows the numerical results for 99 steps, the red line (small dashes) shows the uniform approximation (43) and the green line (large dashes) shows the WKB approximation,

Standard WKB (each turning point considered separately)
is not good for small incident angles due to
merging of turning points!

Comparison with exact solution

$$u(x) = \frac{u_0}{2} (1 + \tanh(x))$$

$$h^2 \frac{d^2 \eta_1}{dx^2} + [q_2 \tanh^2(x) + q_1 \tanh(x) + q_0] \eta_1 = 0$$

$$q_2 = \frac{u_0}{2} \left(\frac{u_0}{2} - ih \right), \quad q_1 = u_0 \left(\frac{u_0}{2} - E \right), \quad q_0 = \left(\frac{u_0}{2} - E \right)^2 - p_y^2 + ih \frac{u_0}{2}$$

By substitution:

$$\xi = (1 - \tanh(x))/2$$

$$4\xi^2(1 - \xi)^2 \frac{d^2 \eta_1}{d\xi^2} + 4\xi(\xi - 1)(2\xi - 1) \frac{d\eta_1}{d\xi} + h^{-2} [q_2(1 - 2\xi)^2 + q_1(1 - 2\xi) + q_0] \eta_1 = 0.$$

Exact solution via hypergeometric function

For above-barrier scattering the exact solution reads

$$\eta_1 = c_1 \xi^{ip_1/2h} (1 - \xi)^{ip_2/2h} {}_2F_1(a, b, c; \xi) \\ + c_2 \xi^{-ip_1/2h} (1 - \xi)^{-ip_2/2h} {}_2F_1(1 - a, 1 - b, 2 - c; \xi)$$

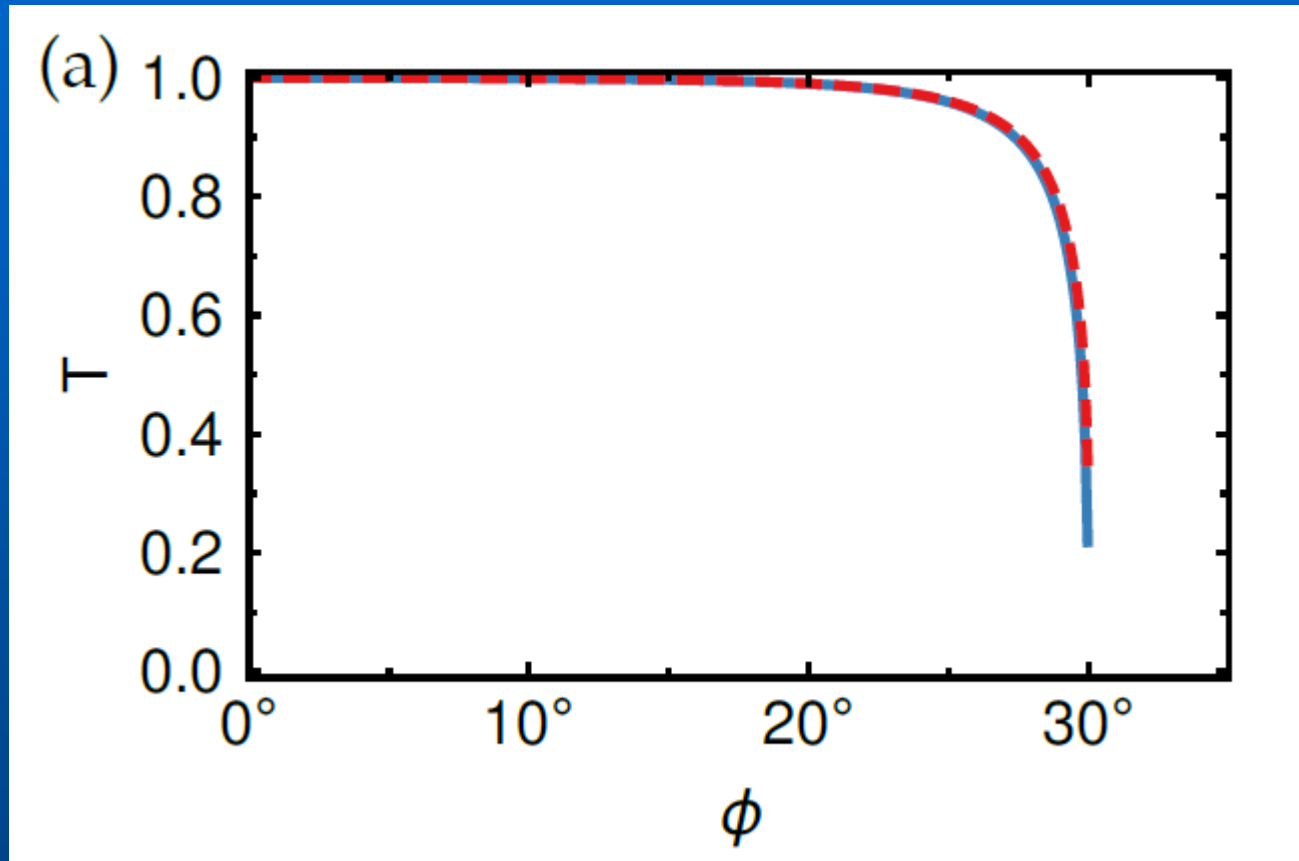
$$a = 1 + \frac{ip_1}{2h} + \frac{ip_2}{2h} + \frac{iu_0}{2h}, \quad b = \frac{ip_1}{2h} + \frac{ip_2}{2h} - \frac{iu_0}{2h}, \quad c = 1 + \frac{ip_1}{h}$$

$$p_1 = \sqrt{(u_0 - E)^2 - p_y^2}$$

$$p_2 = \sqrt{E^2 - p_y^2}$$

$$t^{(a)} = \sqrt{\frac{p_1}{p_2}} \sqrt{\frac{E - u_0 - p_1}{E - p_2}} \frac{\Gamma(1 - a)\Gamma(1 - b)}{\Gamma(2 - c)\Gamma(c - a - b)}$$

Comparison with exact solution



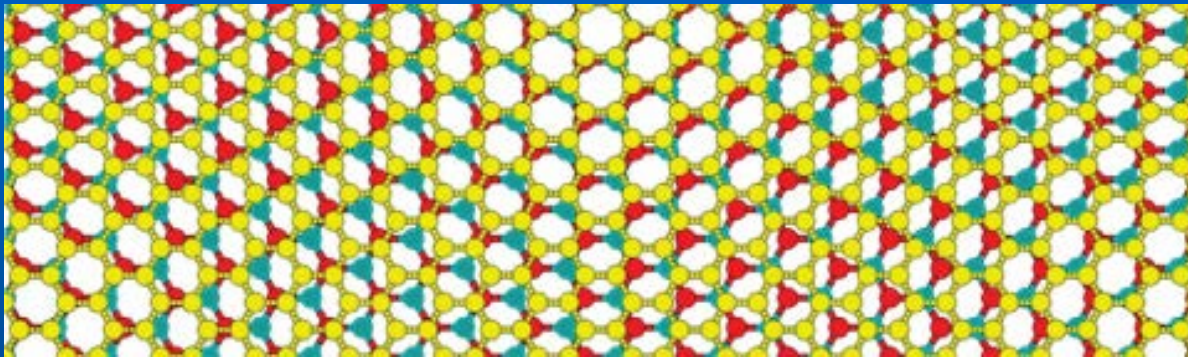
$$T = |t|^2 \quad \hbar = 0.3, \tilde{E} = 2 \text{ and } l_1/l = 2$$

Blue - exact, red dashed - semiclassical

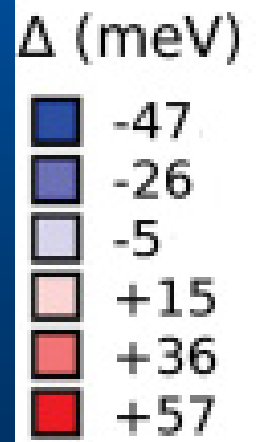
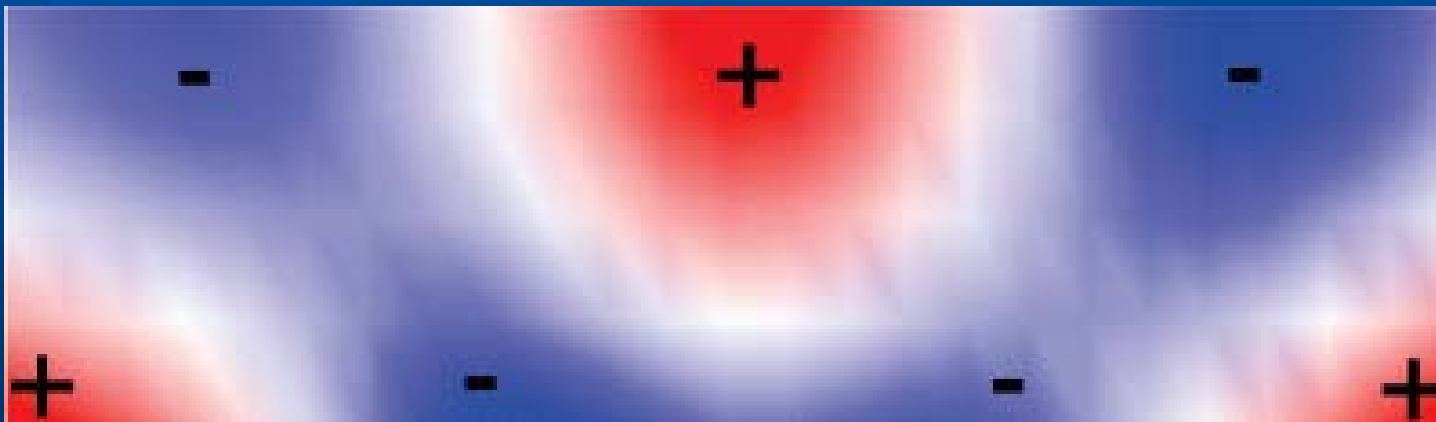
Zero-mass lines

Motivation I: Graphene on hBN

Sachs, Wehling, MIK, Lichtenstein, PRB 84, 195414 (2011)



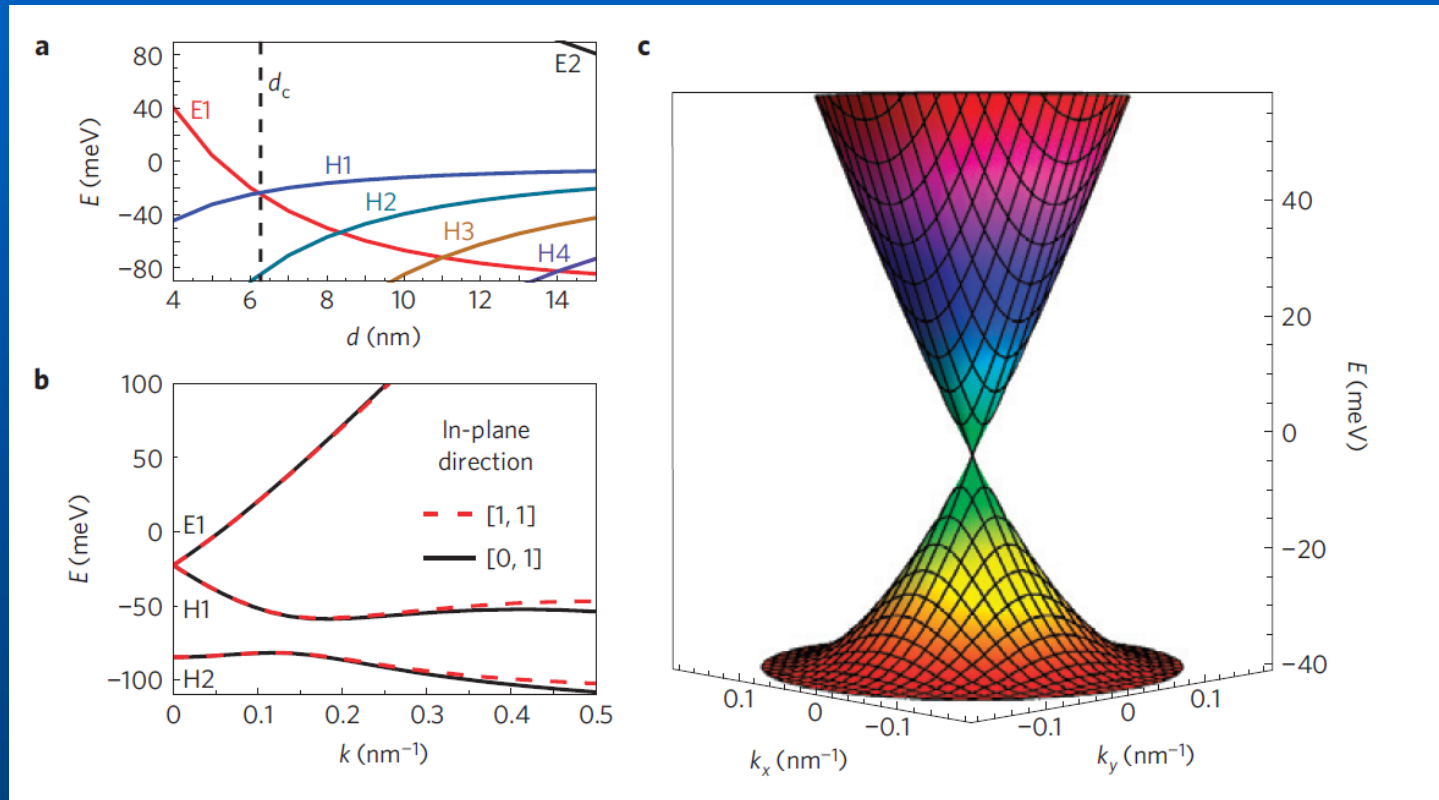
Moiré pattern due to a lattice mismatch



Oscillating energy gap with zero-mass lines

Zero-mass lines II

Motivation II: Quantum wells CdTe/HgTe/CdTe
Molenkamp group, Nature Phys. 7, 418 (2011)



Nonuniform thickness leads to oscillating mass term

Linear dispersion modes

Straight zero-mass line ($y=0$)

$$\hat{H} = \sigma_x \hat{p}_x + \sigma_y \hat{p}_y + \sigma_z m(y)$$

Try the solution $\Psi = e^{ip_x x} \chi(y)$

$$\chi = \frac{1}{\sqrt{2}} \begin{pmatrix} 1 \\ 1 \end{pmatrix} \eta_1 + \frac{1}{\sqrt{2}} \begin{pmatrix} 1 \\ -1 \end{pmatrix} \eta_2$$

$$\begin{pmatrix} p_x - E & \partial_y + m \\ \partial_y - m & p_x + E \end{pmatrix} \begin{pmatrix} \eta_1 \\ \eta_2 \end{pmatrix} = 0$$

Linear-dispersion mode
(LDM)

$$E = -p_x$$

$$\eta_1 = 0$$

$$\eta_2(y) = \exp \left[- \int_0^y dy' m(y') \right]$$

Allowed if m is positive for positive y and negative for negative y

Well known “zero modes” in 1D (supersymmetric QM, fractional charge and solitons in polyacetylene, etc).

Tunneling between zero-mass lines

LDM as models for counterpropagating edge states in TI, QHE, SQHE...

$$m(y) = y^2 - a^2$$

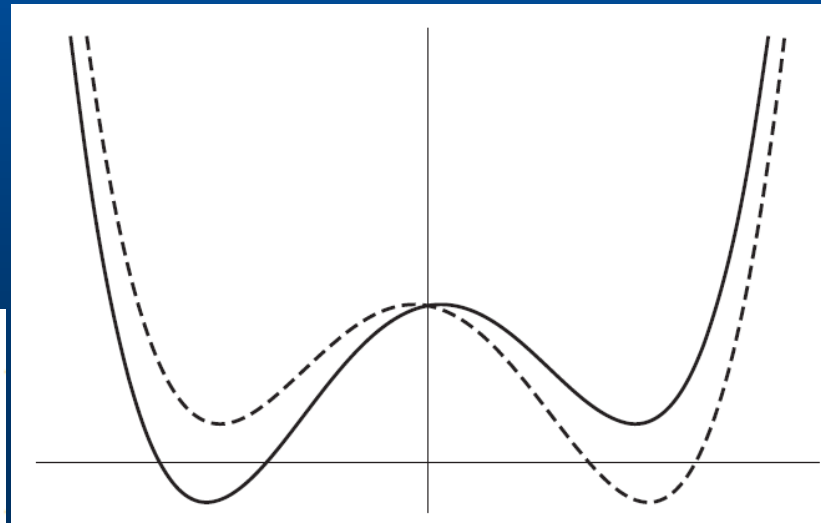
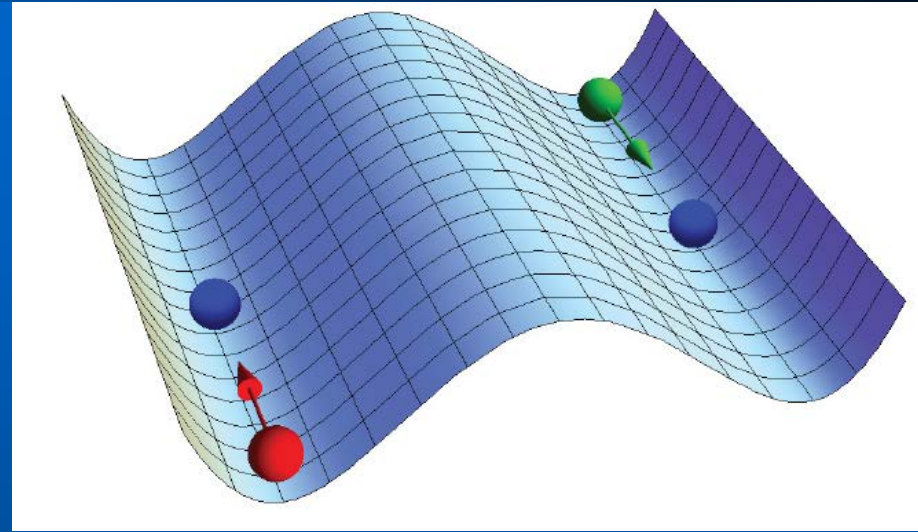
$$[-\partial_y^2 + m(y)^2 + m'(y)]\eta_1 = \lambda\eta_1$$

$$[-\partial_y^2 + m(y)^2 - m'(y)]\eta_2 = \lambda\eta_2$$

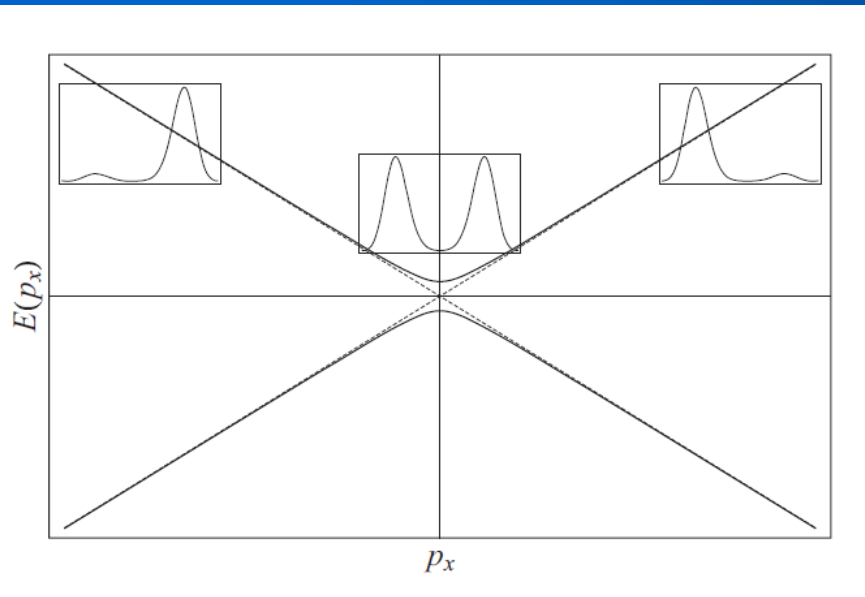
Effective potentials

$$v_1(y) = m(y)^2 + m'(y) = (y^2 - a^2)^2 + 2y$$

$$v_2(y) = m(y)^2 - m'(y) = (y^2 - a^2)^2 - 2y$$



Tunneling between zero-mass lines II



Tunneling splitting

$$2|p_y| = 2\sqrt{\frac{a}{\pi}} \exp(-4a^3/3)$$

General case, ZML at $y = a_1, a_2$

proportional to $\exp\left[-\int_{a_1}^{a_2} |m(y)| dy\right]$

It does not matter whether $m(y)$ is symmetric or not – you always have a tunneling (in contrast with the standard two-well problem), due to existence of zero mode for any $m(y)$, $p_x=0$ (supersymmetry)

Tunneling between edges determines accuracy of quantization in QHE (QSHE) in ideal situation (zero temperature, etc.)

Bent zero-mass line

Parametrization of the line

$$\{x, y\} = \mathbf{R}(\tau)$$

$$|\mathbf{R}'(\tau)| = 1$$

New variables near the line

$$\{x, y\} = \mathbf{R}(\tau) + \xi \mathbf{n}(\tau)$$

τ - coordinate along the line, ξ - normal to the line

Jacobian

$$J = \frac{D(x, y)}{D(\tau, \xi)} = 1 - k(\tau)\xi$$

k - curvature

$$\tilde{\Psi} = \sqrt{1 - k(\tau)\xi} \Psi$$

$$\int_V d\tau d\xi (\tilde{\Psi}^\dagger \tilde{\Psi}) = 1$$

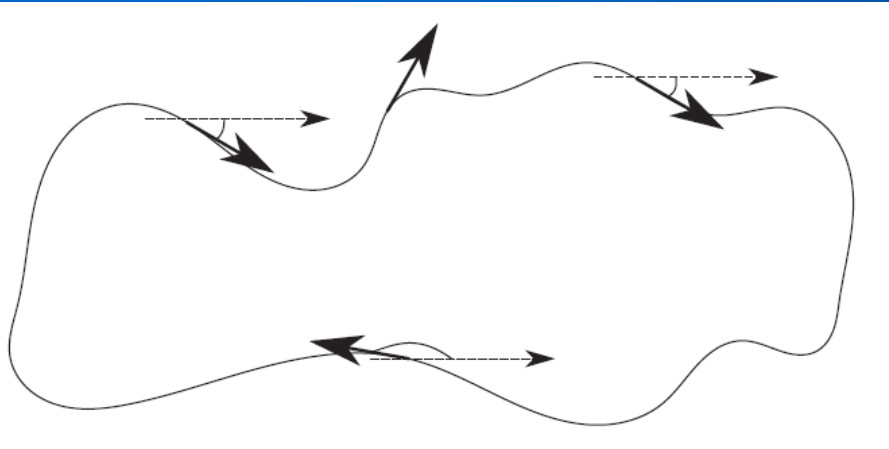
$$\hat{H} \tilde{\Psi} = E \tilde{\Psi}$$

The new Hamiltonian
(exact)

$$\hat{H} = \frac{\sigma \mathbf{R}'(\tau)}{1 - \xi k(\tau)} \hat{p}_\tau - i\sigma \mathbf{n}(\tau) \frac{\partial}{\partial \xi} + \sigma_z m$$

$$- \frac{ik\sigma \mathbf{n}(\tau)}{2[1 - \xi k(\tau)]} - \frac{i\sigma \mathbf{R}'(\tau)\xi k'(\tau)}{2[1 - \xi k(\tau)]^2}$$

Bent zero-mass line II



Smooth line: $|m'_\tau| \ll |m'_\xi|$

$$\hat{H} \simeq \hat{H}_0 + \hat{H}_1$$

$$\hat{H}_0 = \sigma \mathbf{R}'(\tau) \hat{p}_\tau - i \sigma \mathbf{n}(\tau) \frac{\partial}{\partial \xi} + \sigma_z m,$$

$$\hat{H}_1 = \sigma \mathbf{R}'(\tau) \xi k(\tau) \hat{p}_\tau - \frac{ik}{2} \sigma \mathbf{n}(\tau).$$

We use adiabatic approximation and construct semiclassics

Symbol of the operator
in adiabatic approximation

$$\left[\sigma \mathbf{R}'(\tau) p_\tau - i \sigma \mathbf{n}(\tau) \frac{\partial}{\partial \xi} + \sigma_z m \right] \chi(p_\tau, \tau)$$

$$= L_0(p_\tau, \tau) \chi(p_\tau, \tau).$$

Quantization rule for the bent line

Quantization condition
 n integer, w winding #

$$\frac{1}{2\pi} \oint p_\tau d\tau - \frac{E}{2\pi} \oint \langle \tilde{\chi}_1 \xi \chi_2 \rangle_\xi k(\tau) d\tau = n - \frac{w}{2}$$

$$p_\tau = \pm \sqrt{E^2 - \lambda(\tau)}, \quad \lambda(\tau) = L_0^2(p_\tau = 0, \tau)$$

The linear dispersion mode, line length l

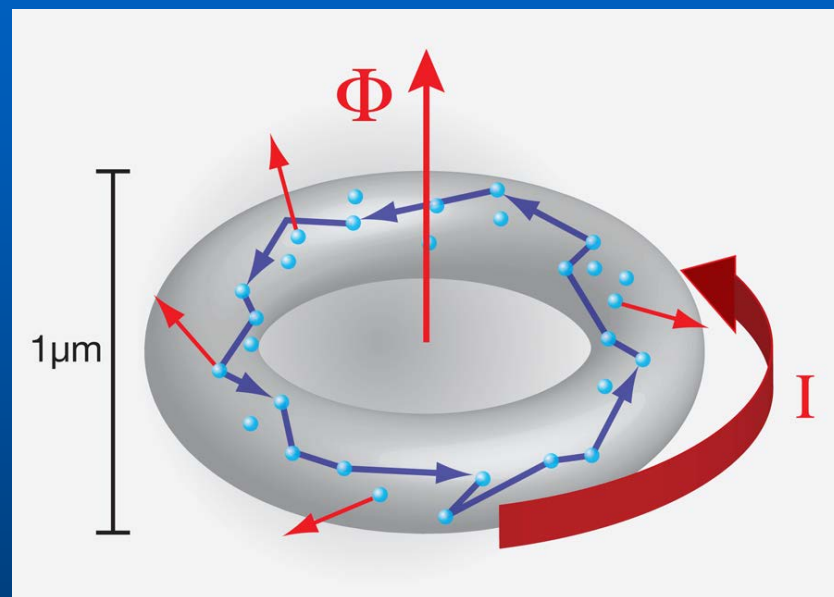
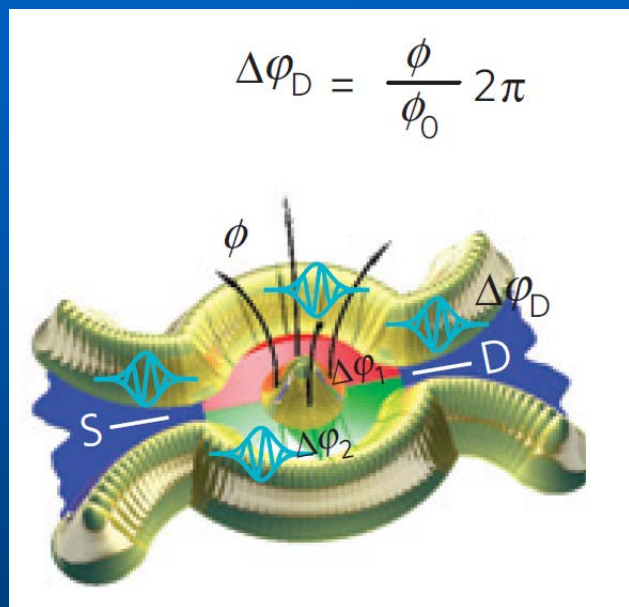
$$E_n = -\frac{2\pi}{l} \left(n - \frac{w}{2} \right) + \frac{2\pi n}{l^2} \oint \langle \tilde{\chi}_1 \xi \chi_2 \rangle_\xi k(\tau) d\tau$$

$$\langle \tilde{\chi}_1 \xi \chi_2 \rangle_\xi = -\frac{N^2(\tau)}{2} \int_{-\infty}^{\infty} \xi \exp \left[-2 \int_0^\xi d\xi' m(\tau, \xi') \right] d\xi$$

$$N(\tau) = \left\{ \int_{-\infty}^{\infty} \exp \left[-2 \int_0^\xi d\xi' m(\tau, \xi') \right] d\xi \right\}^{-1/2}$$

Aharonov-Bohm effect and spectral flow

Persistent current in a ring



If the flux through the ring is integer (in units of flux quantum) the spectrum returns to the initial point

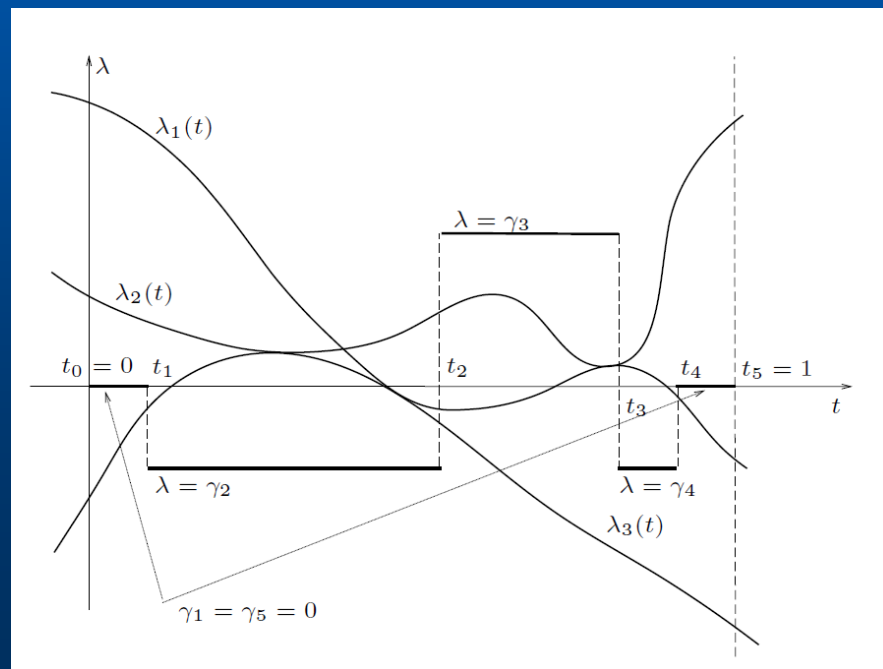
Aharonov-Bohm effect and spectral flow II

Dirac fermions: does coincidence of the spectrum means coincidence of each eigenvalue separately?

No, if the spectrum is from $-\infty$ to $+\infty$ (e.g., $n \rightarrow n+1$, n integer)
For Dirac fermions – the situation may be nontrivial!!!

$$\text{sf}\{B_t\} = \sum_{j=1}^n m_j \text{sign}(\gamma_j - \gamma_{j+1})$$

of eigenvalues crossing some value from below to above minus
of eigenvalues crossing some value from above to below



Aharonov-Bohm effect for zero-mass loop

Add vector potential

$$\hat{H} = -\frac{i\boldsymbol{\sigma}R'(\tau)}{\sqrt{1-\xi k(\tau)}} \frac{\partial}{\partial \tau} \frac{1}{\sqrt{1-\xi k(\tau)}} - i\boldsymbol{\sigma}n(\tau) \frac{\partial}{\partial \xi} - \frac{ik\boldsymbol{\sigma}n(\tau)}{2(1-\xi k(\tau))} - \boldsymbol{\sigma}A + \sigma_z m .$$

Quantization condition

$$E \left(l + \oint G(\tau) k(\tau) d\tau \right) = 2\pi \left(n + \frac{1}{2} \right) + B \left(S + \oint G(\tau) d\tau \right)$$

Magnetic flux

$$\Phi = B \left(S + \oint G(\tau) d\tau \right)$$

$$G(\tau) := 2 \langle \tilde{\chi}_{01} \xi \chi_{02} \rangle_{\xi}$$

$$El = 2\pi(n + 1/2) + \Phi + \dots \quad \text{When flux grows it works like } n \rightarrow n+1$$

Aharonov-Bohm effect and spectral flow in graphene rings

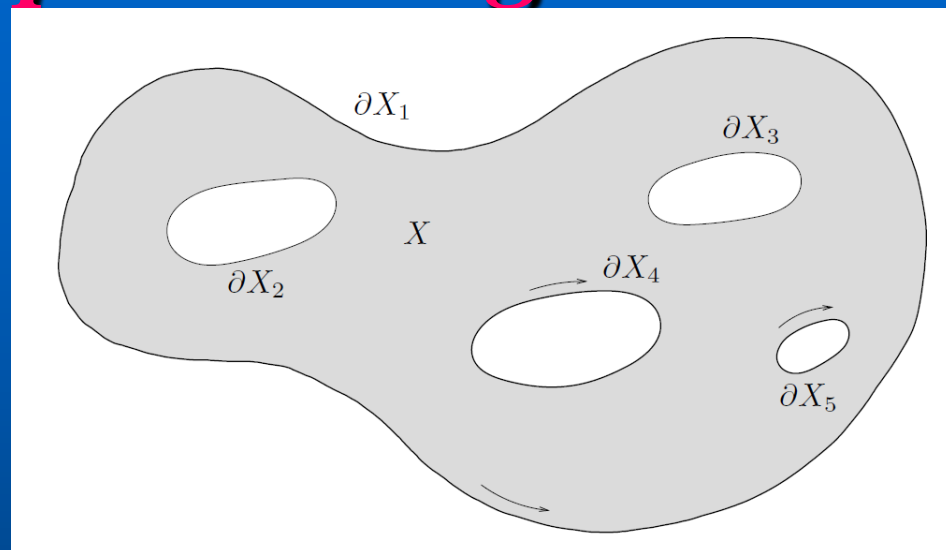
Consequences of non-zero spectral flow: positron (hole) states will move to electron region (or vice versa) – creation of e-h pairs from vacuum by adiabatically slow increasing magnetic field

At any Fermi energy, at some flux, one of eigenvalues will coincide with the Fermi energy – many-body instabilities, etc.

Conditions of nonzero spectral flow for massless Dirac fermions (M. Prokhorova 2011, MIK & V. Nazaiinskii 2012): depend on boundary conditions

Aharonov-Bohm effect and spectral flow in graphene rings II

Geometry of the sample

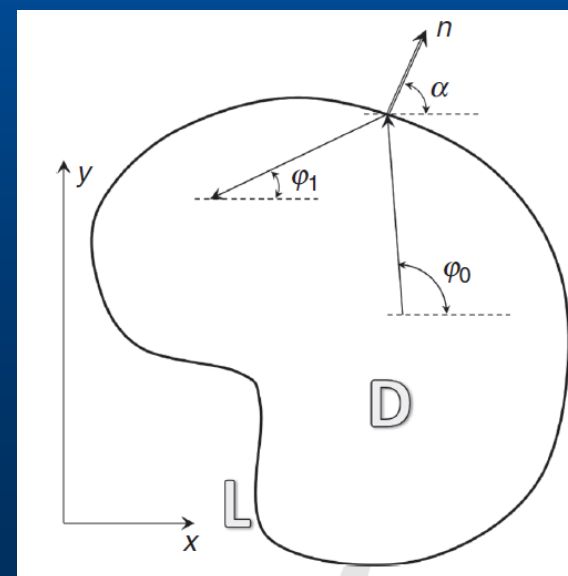


Berry-Mondragon boundary condition

$$\frac{\psi_2}{\psi_1} = iB \exp(i\alpha(s))$$

(mass opening at the Boundary)

B is nonzero real number



Aharonov-Bohm effect and spectral flow in graphene rings III

“gauge transformation” $D_0 \rightarrow \mu D_0 \mu^{-1}$

Theorem 1. *The spectral flow of the family (2) is given by the formula*

$$\text{sf } D_t = \text{wind}_{\partial^+ X} \mu, \quad (3)$$

where $\partial^+ X$ is the part of ∂X where $B > 0$ and

$$\text{wind}_{\partial^+ X} \mu = \frac{1}{2\pi i} \oint_{\partial^+ X} \frac{d\mu}{\mu}$$

is the winding number of the restriction of the function μ to $\partial^+ X$. (The set $\partial^+ X$ is a union of finitely many circles; when defining the winding number, the positive sense of any of these circles is the one for which the domain X remains to the left when moving along the circle.)

Spectral flow = number of fluxes through the holes with positive B (flux through the external boundary is taken with the opposite sign)

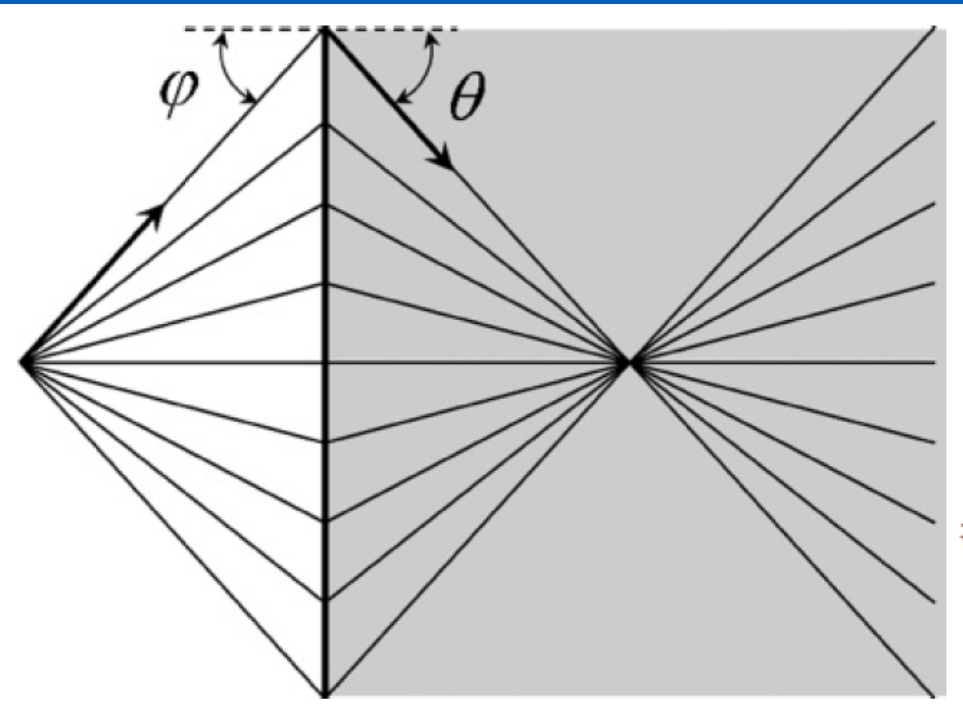
Aharonov-Bohm effect and spectral flow in graphene rings IV

The way of realization: ring with opposite signs of masses at inner and outer boundaries (chemically functionalized graphene; quantum wells CdTe/HgTe/CdTe with varying width; magnetic spots with different signs of magnetization at the surface of 3D topological insulator)... and you will see vacuum reconstruction and other nice stuff

In graphene: the most probably, valley polarization (electrons \rightarrow holes in valley K and holes \rightarrow electrons for valley K')

Klein tunneling and Veselago lensing

If refractive index is negative the flat interface works like lens
(V.S. Veselago, 1968)



Group velocity $\vec{v}_g = \pm v \frac{\vec{k}}{k}$

In electron region:

$$\vec{k} = k(\cos \varphi, \sin \varphi) \quad \vec{v}_e = v(\cos \varphi, \sin \varphi)$$

In hole region:

$$\vec{v}_h = v(\cos \theta', \sin \theta') \quad \vec{q} = -q(\cos \theta', \sin \theta')$$

$$\theta' = -\theta$$

$$\frac{\sin \theta'}{\sin \varphi} = -\frac{k}{q} \equiv n$$

is negative

Graphene with p-n junction as electronic metamaterial

Cheianov, Fal'ko, Altshuler, Science 315, 1252 (2007)

Veselago lens for massless Dirac fermions

Reijnders & MIK, Phys. Rev. B 95, 115310 (2017)

Green function

$$[v_F \boldsymbol{\sigma} \cdot \hat{\mathbf{p}} + U(\mathbf{x})1_2]G(\mathbf{x}, \mathbf{x}_0) = EG(\mathbf{x}, \mathbf{x}_0) + \delta(\mathbf{x} - \mathbf{x}_0)1_2$$

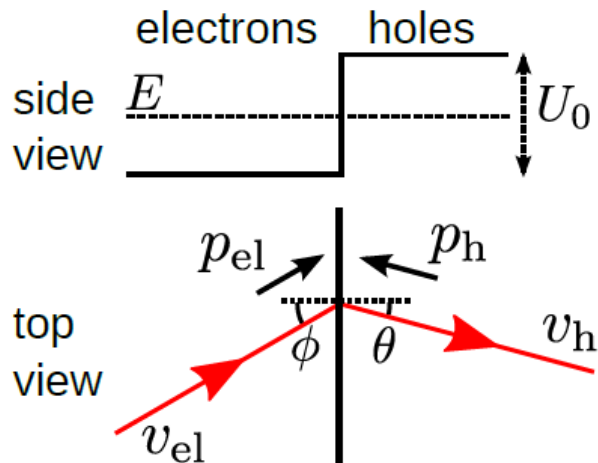
Wave function from initially polarized source

$$\Psi(\mathbf{x}) = G(\mathbf{x}, \mathbf{x}_s) \begin{pmatrix} \alpha_1 \\ \alpha_2 \end{pmatrix}$$

U is just a potential step

$$U(\mathbf{x}) = U(x) = U_0 \Theta(x)$$

Source: $\mathbf{x}_s = (x_s, 0)$



$$\frac{\sin \phi}{\sin \theta} = -\frac{p_h}{p_e} = -\frac{U_0 - E}{E} \equiv n$$

Veselago lens for Dirac fermions II

Classical Hamiltonian

$$H_{cl}^{\pm} = \pm|\mathbf{p}| + U(\mathbf{x})$$

Classical action

$$S_{np}(p_y, x, y) = -x_s \sqrt{E^2 - p_y^2} - x \sqrt{(E - U_0)^2 - p_y^2} + y p_y$$

Classical trajectories

$$\begin{aligned} y &= -x_s \frac{p_y}{\sqrt{E^2 - p_y^2}} - x \frac{p_y}{\sqrt{(E - U_0)^2 - p_y^2}} \\ &= -x_s \tan \phi + x \tan \theta. \end{aligned}$$

Singular points (caustics): $\partial^2 S_{np} / \partial p_y^2$ vanishes

They form the lines (caustics) where density of trajectories is divergent

Veselago lens for Dirac fermions III

$$x_{\text{cst}} = -x_s \frac{E^2}{(E - U_0)^2} \frac{((E - U_0)^2 - p_y^2)^{3/2}}{(E^2 - p_y^2)^{3/2}}$$

$$y_{\text{cst}}(x_{\text{cst}}) = \pm \sqrt{\frac{(x_{\text{cst}}^{2/3} - x_{\text{cusp}}^{2/3})^3}{n^2 - 1}}, \quad x_{\text{cusp}} = -|n|x_s$$

Cheianov, Fal'ko & Altshuler, 2007

Caustics separated the regions where each point belong to one trajectory and where it belongs to 3 trajectories

Exact Green function (without evanescent waves)

$$G(\mathbf{x}, \mathbf{x}_0) = \frac{i}{4\pi h^2} \int_{-p_{y,\text{max}}}^{p_{y,\text{max}}} \begin{pmatrix} e^{i\phi/2} e^{-i\theta/2} & e^{-i\phi/2} e^{-i\theta/2} \\ e^{i\phi/2} e^{i\theta/2} & e^{-i\phi/2} e^{i\theta/2} \end{pmatrix} \times \frac{1}{\cos[(\phi + \theta)/2]} e^{iS_{np}(p_y, x, y)/h} dp_y, \quad (\text{A25})$$

where the classical action $S_{np}(p_y, x, y)$ is given by

$$S_{np}(p_y, x, y) = -x_0 \sqrt{E^2 - p_y^2} - x \sqrt{(E - U_0)^2 - p_y^2} + (y - y_0)p_y. \quad (\text{A26})$$

Caustics separate regions with and without interference patterns

Veselago lens for Dirac fermions IV

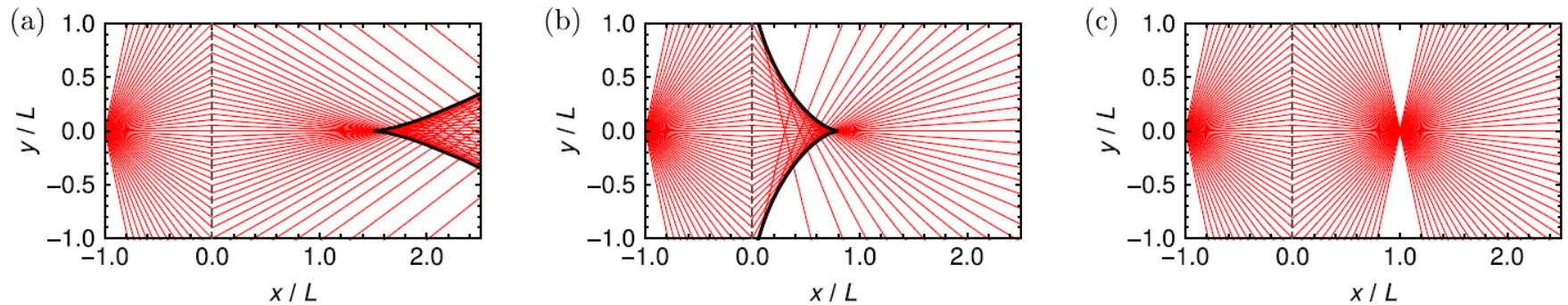


FIG. 1. The classical trajectories (red lines) for massless Dirac fermions that are emitted by a point source and are incident on an n - p junction at $x = 0$ (dashed gray line). We see that the junction focusses the particles. The solid black line indicates the caustic, which is the envelope of the classical trajectories, and separates the region where each point lies on a single trajectory from the region where each point lies on three trajectories. It consists of twofold lines meeting into a cusp point at $(x_{\text{cusp}}, 0)$. (a) For $U_0 > 2E$, the cusp point $x_{\text{cusp}} > -x_s$ is the left-most point of the caustic. (b) When $U_0 < 2E$, the cusp point $x_{\text{cusp}} < -x_s$ is the right-most point of the caustic. (c) For $U_0 = 2E$, all trajectories are focused into a single point.

$U_0 = 2E$ is an exceptional case, $n = -1$, ideal focus
(the caustics shrink to a single point)

Interference patterns

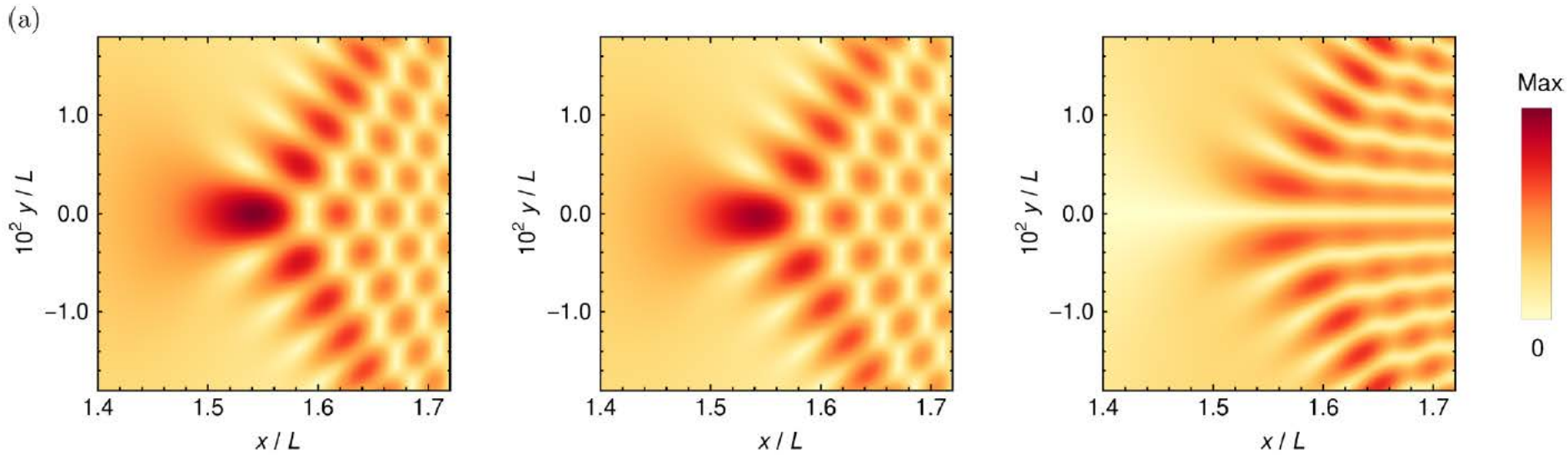
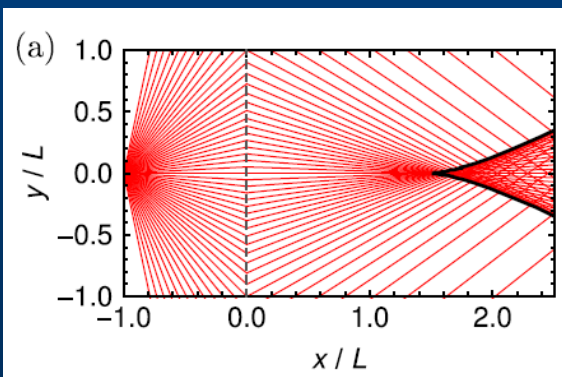


FIG. 7. The density $\|\Psi\|$ for the dimensionless parameters $U_0 = 2.5$ and $h = 0.000639$. For graphene, these numbers correspond to $E = 100$ meV, $U_0 = 250$ meV, and $L = 10^4$ nm. (a) The exact result obtained by numerically evaluating the exact wave function (16). (b)

The left, middle, and right panels correspond to three different polarizations (α_1, α_2) , to wit $(1,1)/\sqrt{2}$; $(1,0)$ and $(1,-1)/\sqrt{2}$



$$U_0 > 2E$$

Pseudospin polarization and symmetry breaking

$$S_{np}(x, -y, -p_y) = S_{np}(x, y, p_y)$$

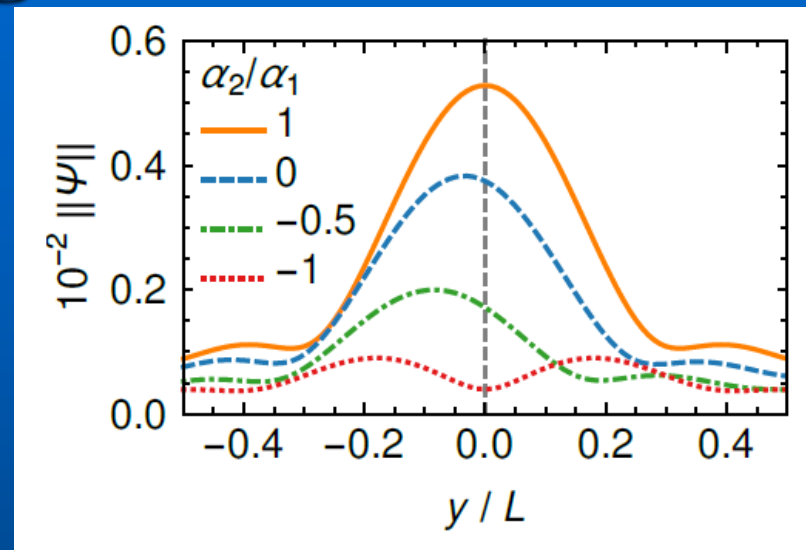
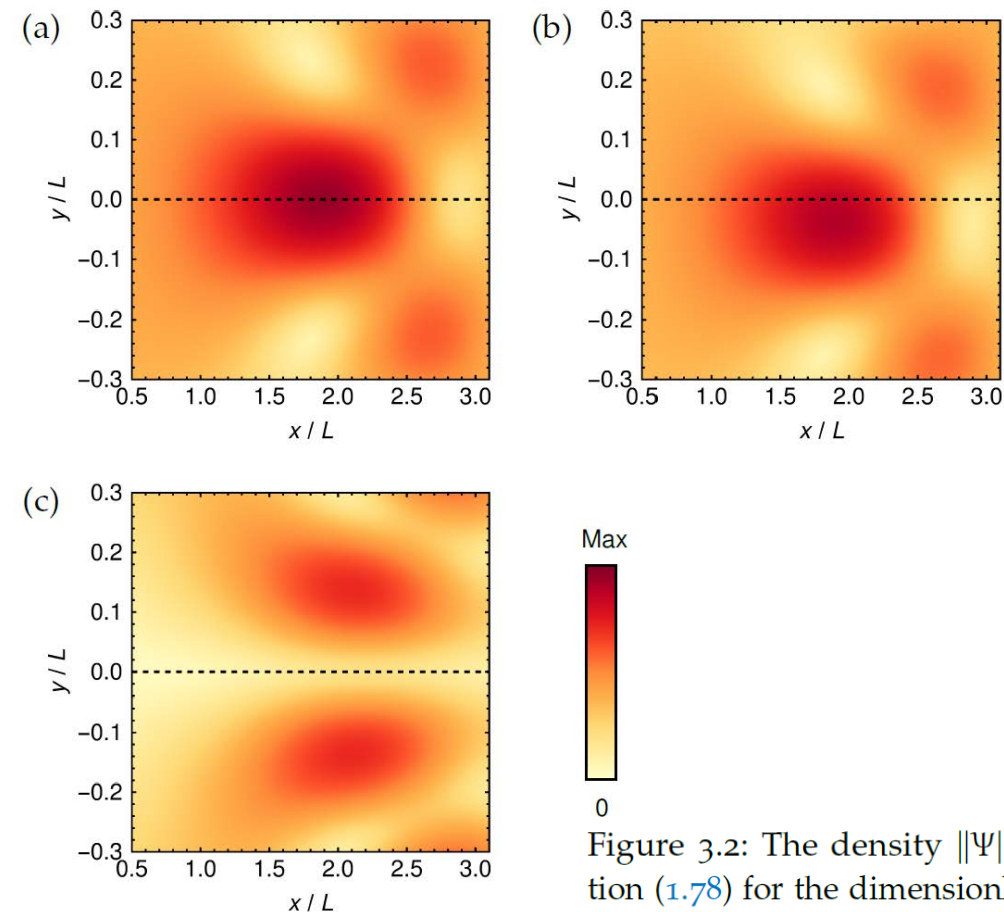
$$G(x, -y, x_0, -y_0) = \sigma_x G(x, y, x_0, y_0) \sigma_x$$

$$\begin{aligned} \|\Psi(x, -y)\|^2 &= \left\| \sigma_x G(x, y, x_s, 0) \sigma_x \begin{pmatrix} \alpha_1 \\ \alpha_2 \end{pmatrix} \right\|^2 \\ &= \left\| G(x, y, x_s, 0) \begin{pmatrix} \alpha_2 \\ \alpha_1 \end{pmatrix} \right\|^2. \end{aligned}$$

This is equal to $\|\Psi(x, y)\|^2$ only if $\alpha_1 = \pm \alpha_2$

(Pseudo)spin polarization breaks the mirror symmetry!

Pseudospin polarization and symmetry breaking II



$X = X_{\text{cusp}}$

Figure 3.2: The density $\|\Psi\|$ computed by numerically evaluating the exact wavefunction (1.78) for the dimensionless parameters $U_0 = 2.5$ and $h = 0.0639$. For graphene, these numbers correspond to $E = 100$ meV, $U_0 = 250$ meV and $L = 100$ nm. We consider three different polarizations. (a) For $(\alpha_1, \alpha_2) = (1, 1)/\sqrt{2}$, the density is symmetric about the x -axis. (b) When $(\alpha_1, \alpha_2) = (1, 0)$, this symmetry is no longer there and the maximum lies at $y < 0$. (c) For $(\alpha_1, \alpha_2) = (1, -1)/\sqrt{2}$, the density is symmetric again, but the central resonance has disappeared. The maximum of the color scale equals (a) 70, (b) 55 and (c) 22.

WKB approximation

$$\Psi(x, y) = \iint G(x, y, x_0, y_0) J(x_0, y_0) dx_0 dy_0$$

$$J(x, y) = \begin{pmatrix} \alpha_1 \\ \alpha_2 \end{pmatrix} \delta(x + L) \delta(y)$$

Green's function

$$G(x, y, x_0, y_0) \propto \underbrace{\int \frac{dp_y}{\cos \frac{\phi + \theta}{2}} \begin{pmatrix} e^{i(\phi - \theta)/2} & e^{-i(\phi + \theta)/2} \\ e^{i(\phi + \theta)/2} & e^{-i(\phi - \theta)/2} \end{pmatrix}}_{\text{Amplitude } f(p_y)} \underbrace{e^{iS_{np}(x, y, x_0, y_0)/h}}_{\text{Action } S_{np}}$$

$$S_{np}(x, y, x_0, y_0) = |x_0| \sqrt{E^2 - p_y^2} - x \sqrt{(U_0 - E)^2 - p_y^2} + (y - y_0) p_y$$

h is small: we need to calculate fastly oscillating integrals

WKB approximation II

$$I(\mathbf{x}, \hbar) = \int_{-\infty}^{\infty} d\eta f(\mathbf{x}, \eta) e^{iS(\mathbf{x}, \eta)/\hbar} \quad \hbar \rightarrow 0$$

Main contribution is from stationary points

$$\left. \frac{\partial S}{\partial \eta_i} \right|_{(\mathbf{x}_0, \eta_0)} = 0, \quad i = 1 \dots n$$

Generic case:

$$\det A(\mathbf{x}_0, \eta_0) \equiv \det \left. \frac{\partial^2 S}{\partial \eta_i \partial \eta_j} \right|_{(\mathbf{x}_0, \eta_0)} \neq 0$$

$$I(\mathbf{x}, \hbar) = (2\pi\hbar)^{n/2} \frac{f(\mathbf{x}_0, \eta_0)}{\sqrt{|\det A(\mathbf{x}_0, \eta_0)|}} e^{i\pi \operatorname{sgn}(A(\mathbf{x}_0, \eta_0))/4} \times e^{iS(\mathbf{x}_0, \eta_0)/\hbar} (1 + \mathcal{O}(\hbar))$$

In QM it corresponds to WKB approximation

Does not work near caustics or cusps!

Airy approximation I

Fold caustics: Airy approximation

$$\left. \frac{\partial S}{\partial \eta} \right|_{(x_0, \eta_0)} = 0, \quad \text{and} \quad \left. \frac{\partial^2 S}{\partial \eta^2} \right|_{(x_0, \eta_0)} = 0$$

Expand to the higher (third) order:

$$\begin{aligned} S(\mathbf{x}, \eta) &= S^{(3)}(\mathbf{x}, \eta) + \mathcal{O}(\beta^4) \\ &= q_0(\mathbf{z}) + q_1(\mathbf{z})\beta + \frac{q_2(\mathbf{z})}{2}\beta^2 + \frac{q_3(\mathbf{z})}{6}\beta^3 + \mathcal{O}(\beta^4) \end{aligned}$$

$$\beta = \eta - \eta_0$$

$$\mathbf{z} = \mathbf{x} - \mathbf{x}_0$$

$$q_0(\mathbf{z}) = a_0 + \langle \mathbf{b}_0, \mathbf{z} \rangle + \mathcal{O}(z^2), \quad q_1(\mathbf{z}) = \langle \mathbf{b}_1, \mathbf{z} \rangle + \mathcal{O}(z^2),$$

$$q_2(\mathbf{z}) = \langle \mathbf{b}_2, \mathbf{z} \rangle + \mathcal{O}(z^2), \quad q_3(\mathbf{z}) = a_3 + \mathcal{O}(z).$$

Airy approximation II

$$\begin{aligned} I(\mathbf{x}, h) &= \int_{-\infty}^{\infty} d\eta f(\mathbf{x}, \eta_0) e^{iS^{(3)}(\mathbf{x}, \eta)/h} + \mathcal{O}(h^{2/3}), \\ &= 2\pi f(\mathbf{x}, \eta_0) \sqrt[3]{\frac{2h}{|q_3|}} \exp \left[\frac{i}{h} \left(q_0 + \frac{q_2^3}{3q_3^2} - \frac{q_1 q_2}{q_3} \right) \right] \\ &\quad \times \text{Ai} \left[\frac{2^{1/3}}{h^{2/3} q_3^{1/3}} \left(q_1 - \frac{q_2^2}{2q_3} \right) \right] + \mathcal{O}(h^{2/3}) \end{aligned}$$

is expressed via Airy function

$$\text{Ai}(u) = \frac{1}{2\pi} \int_{-\infty}^{\infty} \exp \left(\frac{i}{3} t^3 + iut \right) dt$$

Airy approximation III

$$q_0 + \frac{q_2^3}{3q_3^2} - \frac{q_1 q_2}{q_3} = a_0 + \langle \mathbf{b}_0, \mathbf{z} \rangle + \mathcal{O}(z^2),$$

$$\frac{2^{1/3}}{h^{2/3} q_3^{1/3}} \left(q_1 - \frac{q_2^2}{2q_3} \right) = \frac{2^{1/3} \langle \mathbf{b}_1, \mathbf{z} \rangle}{h^{2/3} a_3^{1/3}} + \frac{\mathcal{O}(z^2)}{h^{2/3}}$$

The answer:

$$I(\mathbf{x}, h) = 2\pi f(\mathbf{x}_0, \eta_0) \sqrt[3]{\frac{2h}{|a_3|}} \exp \left[\frac{i}{h} (a_0 + \langle \mathbf{b}_0, \mathbf{z} \rangle) \right] \\ \times \text{Ai} \left(\frac{2 \langle \mathbf{b}_1, \mathbf{z} \rangle}{2^{2/3} h^{2/3} a_3^{1/3}} \right) + \mathcal{O}(h^{2/3})$$

Does not work near cusp!

Pearcey approximation

Near cusp, third derivative disappears as well

$$S(\mathbf{x}, \eta) = S^{(4)}(\mathbf{x}, \eta) + \mathcal{O}(\beta^5) = q_0(\mathbf{z}) + q_1(\mathbf{z})\beta + \frac{q_2(\mathbf{z})}{2}\beta^2 + \frac{q_3(\mathbf{z})}{6}\beta^3 + \frac{q_4(\mathbf{z})}{24}\beta^4 + \mathcal{O}(\beta^5)$$

$$I(\mathbf{x}, \hbar) = f(\mathbf{x}_0, \eta_0) \sqrt[4]{\frac{24\hbar}{|\alpha_4|}} \exp \left[\frac{i}{\hbar} (\alpha_0 + \langle \mathbf{b}_0, \mathbf{z} \rangle) \right] \\ \times P^\pm \left[\sqrt{\frac{6}{\hbar|\alpha_4|}} \langle \mathbf{b}_2, \mathbf{z} \rangle, \sqrt[4]{\frac{24}{\hbar^3|\alpha_4|}} \langle \mathbf{b}_1, \mathbf{z} \rangle \right] + \mathcal{O}(\hbar^{1/2})$$

Pearcey function

$$P^\pm(u, v) = \int_{-\infty}^{\infty} \exp \left(\pm it^4 + iut^2 + ivt \right) dt$$

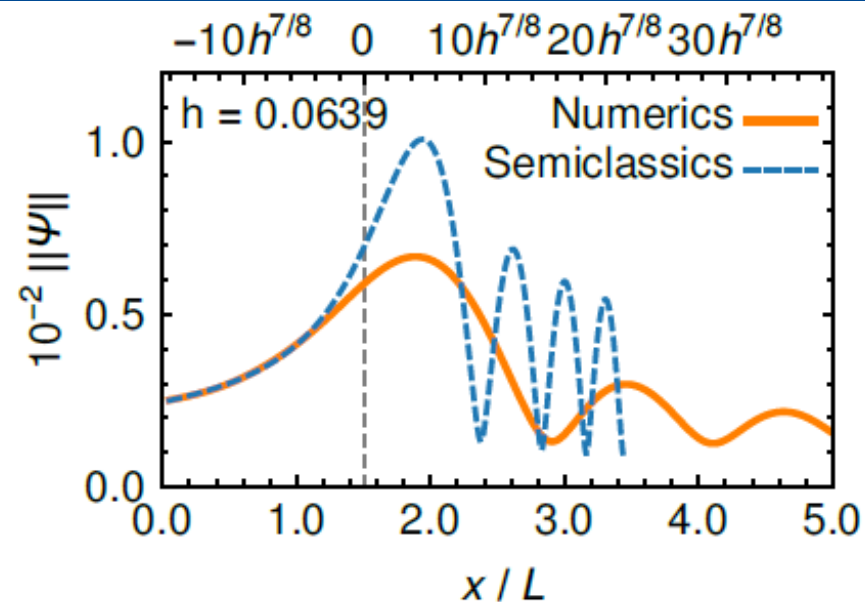
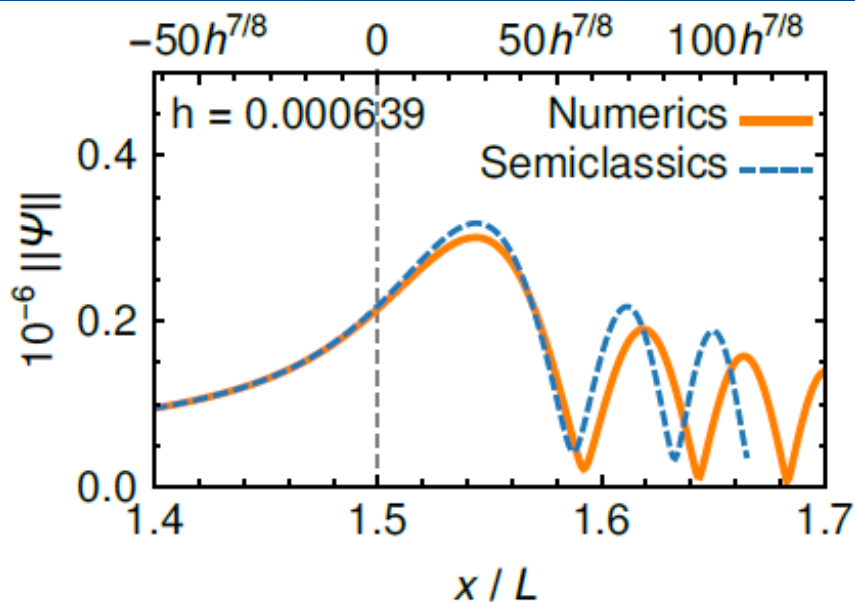
Pearcey approximation II

Expand action up to 4th order around $p_y = 0$ (not at ideal focus)

$$\Psi(x, y) \propto h^{1/4} f(0) P^\pm \left[\sqrt{\frac{6}{h|a_4|}} \frac{x - x_{\text{cusp}}}{U_0 - E}, \sqrt[4]{\frac{24}{h^3|a_4|}} y \right] \left(1 + \mathcal{O}(h^{1/4}) \right)$$

$$P^\pm(u, v) = \int d\eta \exp(\pm i\eta^4 + iu\eta^2 + iv\eta), \quad a_4 = \left. \frac{\partial^4 S_{\text{np}}}{\partial p_y^4} \right|_{\substack{p_y=0, \\ x=x_{\text{cusp}}}}$$

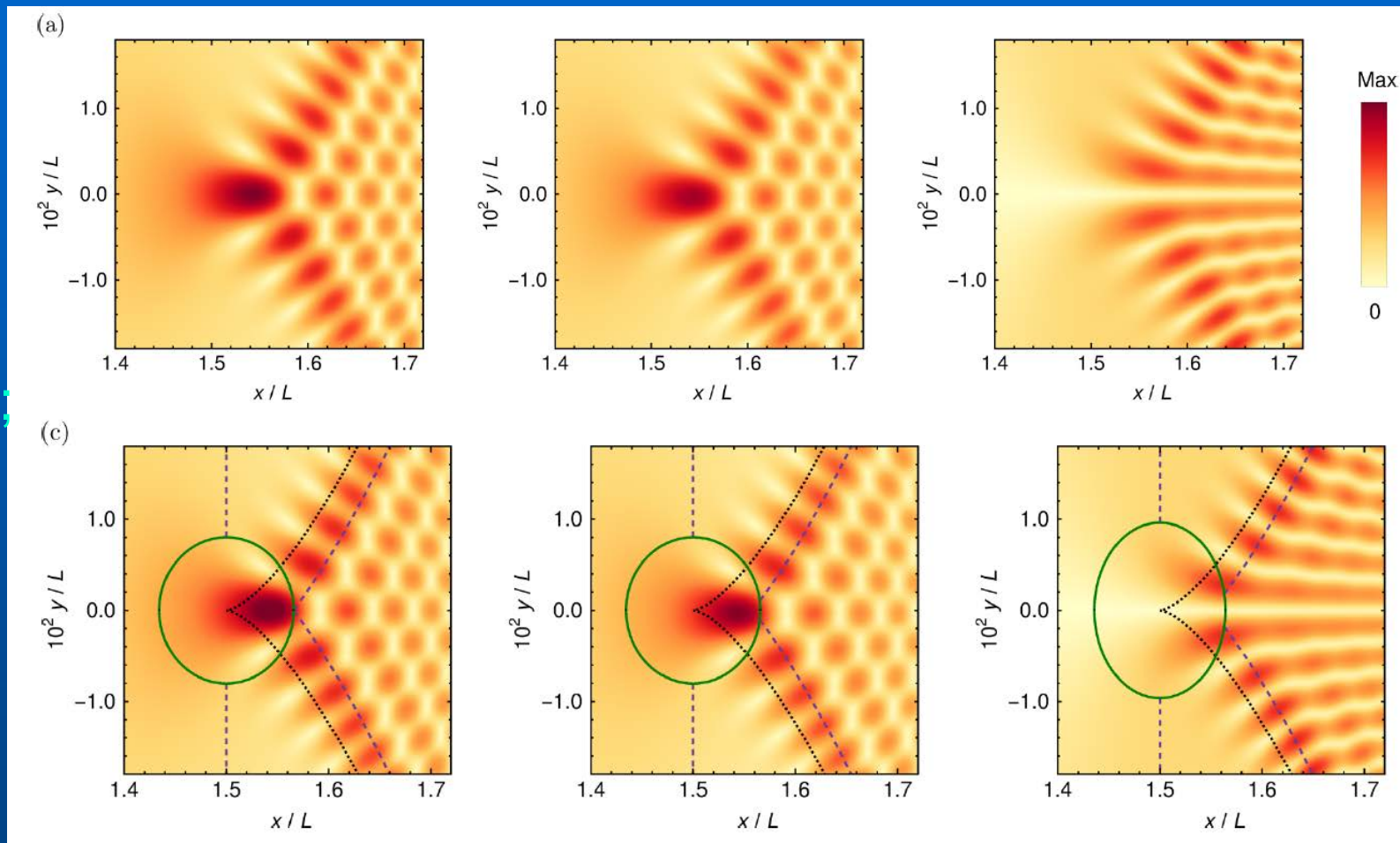
Works only at small h but position of the main maximum is good



Semiclassical approximation

Exact

Pearcey
(in ellipse);
Airy
(between
dashed
lines);
WKB
(outside)



The density $\|\Psi\|$ for the dimensionless parameters $U_0 = 2.5$ and $h = 0.000639$

Asymmetry in y direction

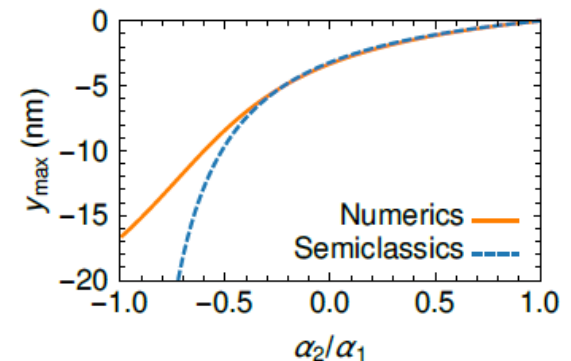
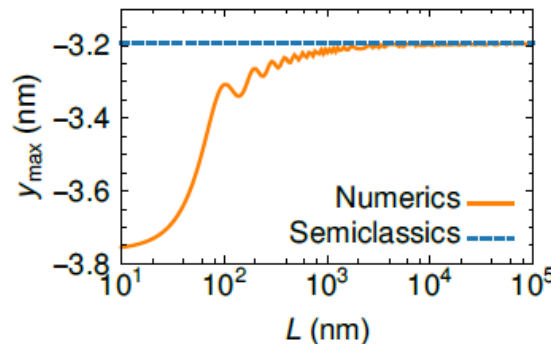
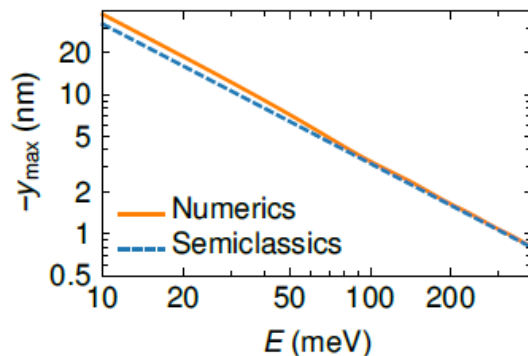
Pearcey function symmetric: include corrections

$$\Psi(x) = \int f(p_y) e^{iS_{np}(x,y,p_y)/\hbar} \approx \int (f(0) + f'(0)p_y) e^{iS_{np}^{(4)}(x,y,p_y)/\hbar} dp_y$$

$$\propto \hbar^{1/4} \left(f(0) P^\pm(\alpha, \beta) + \hbar^{1/4} f'(0) P_\beta^\pm(\alpha, \beta) + \mathcal{O}(\hbar^{1/2}) \right)$$

Expand P^\pm to 2nd order in β , consider the cusp point ($\alpha = 0$)

Maximum of $\|\Psi\|^2$ at $y_{\max} = -\frac{\hbar}{2E} \frac{\alpha_1 - \alpha_2}{\alpha_1 + \alpha_2} \xrightarrow[\text{units}]{\text{restore}} -\frac{\hbar v_F}{2E} \frac{\alpha_1 - \alpha_2}{\alpha_1 + \alpha_2}$

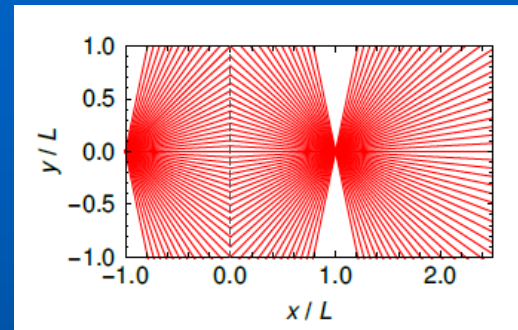


The effects of trigonal warping

Reijnders & MIK, Phys. Rev. B 96, 045305 (2017)

For Dirac fermions and $U_0 = 2E$
ideal focus

It is unstable in view of
catastrophe theory



Trigonal warping: correction to the linear spectrum of graphene

$$E_{\alpha}^{\pm} = \pm \left(|\mathbf{p}| + \alpha \mu |\mathbf{p}|^2 \cos [3(\phi_{\mathbf{p}} + \theta)] \right), \quad \mu \ll 1, \alpha = \pm 1$$

α is opposite for different valleys, θ depends on crystallographic orientation ($\theta = 0$ corresponds to zigzag edges along x-direction)

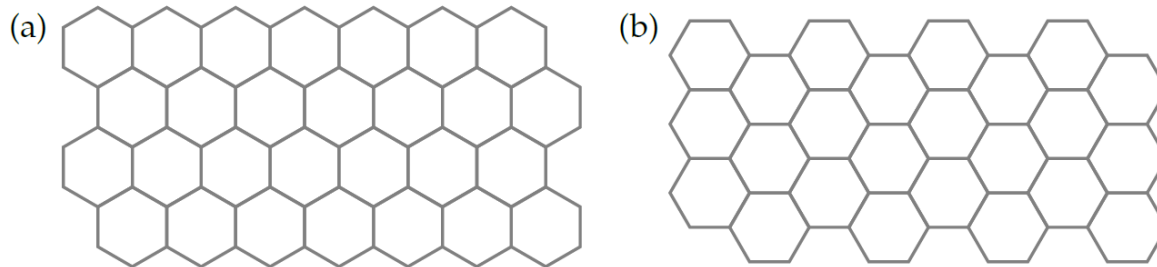


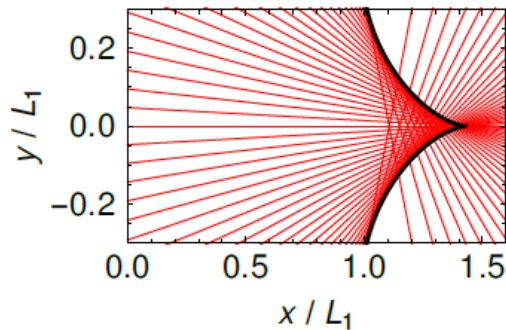
Figure 1.4: (a) Zigzag edges along the x-axis ($\theta = 0$). (b) Armchair edges along the x-axis ($\theta = \pi/6$).

The effects of trigonal warping II

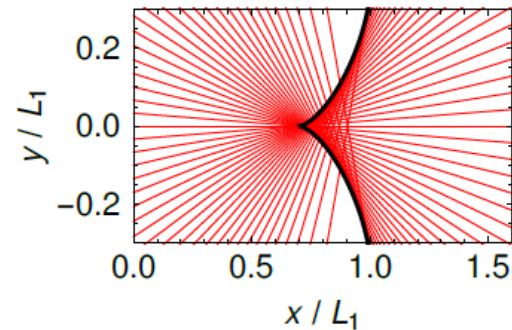
Fate of the ideal focus

Generic orientation θ : ideal focus becomes cusp caustic

$$U_0 = 2E, \theta = 0, \alpha = -1$$

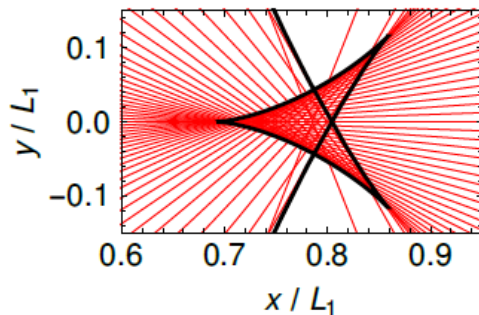


$$U_0 = 2E, \theta = 0, \alpha = 1$$

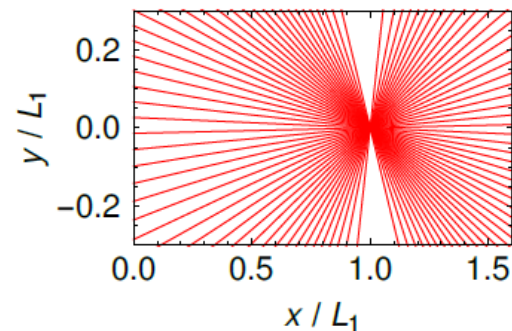


By varying U_0 we obtain a butterfly caustic, not an ideal focus

$$U_0 \lesssim 2E, \theta = 0, \alpha = 1$$



$$U_0 = 2E, \theta = \pi/6$$



Only for $\theta = \pi/6$ the ideal focus at $U_0 = 2E$ remains intact

The effects of trigonal warping III

Veselago lens with trigonal warping produces valley polarization*;
in particular, the maxima of wave function are shifted

*Garcia-Pomar, Cortijo, Nieto-Vesperinas, Phys Rev Lett 100, 236801 (2008)

Semiclassical analysis similar to Dirac case + numerical TB simulations

K. J. A. REIJNDERS AND M. I. KATSNELSON

PHYSICAL REVIEW B **96**, 045305 (2017)

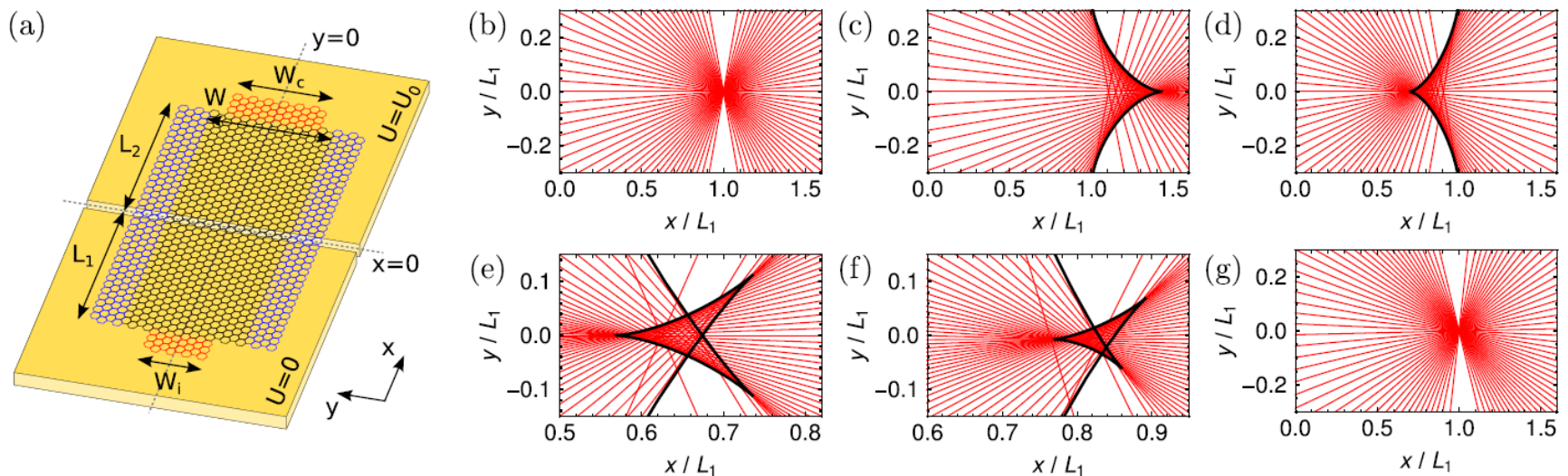


FIG. 1. (a) Simulation setup with an injector and collector lead (red) and drain leads on each side (blue). (b) Classical trajectories for the massless Dirac Hamiltonian at $U_0 = 2E$. (c)–(g) Classical trajectories (red) and caustics (black) for the Hamiltonian including trigonal warping. Unless otherwise indicated, $E = 0.4$ eV. (c) K valley, $U_0 = 0.8$ eV, $\theta = 0$; (d) K' valley, $U_0 = 0.8$ eV, $\theta = 0$; (e) section of the butterfly caustic, K' valley, $E = 0.6$ eV, $U_0 = 1.18$ eV, $\theta = 0$; (f) K' valley, $U_0 = 0.795$ eV, $\theta = \pi/12$; (g) $U_0 = 0.8$ eV, $\theta = \pi/6$.

The effects of trigonal warping IV

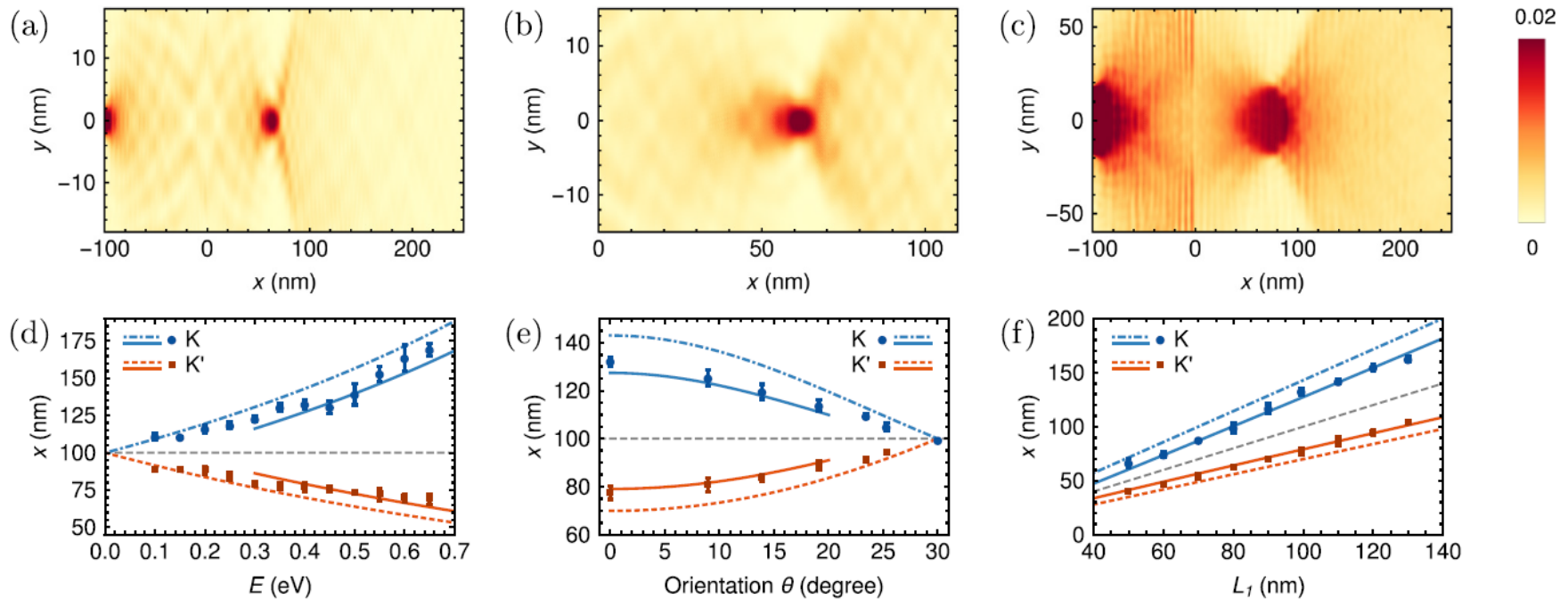


FIG. 2. (a)–(c) Results of the tight-binding simulations with $L_1 = 100$ nm. The density $|\Psi_{av,\alpha}|^2$ is averaged over sublattices and summed over lead modes in valley α . (a) K' valley, $E = 0.6$ eV, $U_0 = 2E$, $W_i = 7.5$ nm; (b) K' valley, $E = 0.6$ eV, $U_0 = 1.18$ eV, $W_i = 7.5$ nm; cf. the classical trajectories in Fig. 1(e); (c) K' valley, $E = 0.4$ eV, $U_0 = 2E$, $W_i = 40$ nm. (d)–(f) Position, on the x axis, of the caustic (dashed and dashed-dotted lines), semiclassical maximum (solid lines), and simulated maximum (symbols) for varying energy E , lattice orientation θ , and L_1 . The dashed gray lines indicate the Dirac result. The parameters equal (e),(f) $E = 0.4$ eV, (d),(f) $\theta = 0$, (d),(e) $L_1 = 100$ nm, (d),(f) $W_i = 40$ nm, and (e) $W_i = 50$ nm. In all cases $U_0 = 2E$.

Semiclassical (Pearcey) approximation works very well; qualitatively, the splitting can be understood just from classical trajectories

Two-dimensional case

Electronic optics in graphene in the semiclassical approximation

Annals of Physics 397 (2018) 65–135

K.J.A. Reijnders^{a,*}, D.S. Minenkov^b, M.I. Katsnelson^a,
S.Yu. Dobrokhotov^{b,c}

$$\hat{H}_\alpha \Psi_\alpha = E \Psi_\alpha, \quad \Psi_\alpha = \begin{pmatrix} \psi_1 \\ \psi_2 \end{pmatrix}$$

$$\hat{H}_\alpha = \begin{pmatrix} U(x) + m(x) & \hat{p}_1 + i\alpha \hat{p}_2 \\ \hat{p}_1 - i\alpha \hat{p}_2 & U(x) - m(x) \end{pmatrix}$$

$$x = (x_1, x_2)$$

$\alpha = -1$ for the K -valley and $\alpha = +1$ for the K' -valley

Only above-barrier case is considered; even this is quite demanding, tunneling problem is extremely difficult

$$(U(x) - E)^2 - m(x)^2 > 0 \text{ for all } x$$

Two-dimensional case II

Scattering problem

$$\Psi_\alpha(x) = A^0 e^{i\langle p^0, x \rangle / \hbar} + \Psi_{\text{scat}, \alpha}(x)$$

$$\lim_{|x| \rightarrow \infty} |x|^{1/2} \left(-i\hbar \frac{\partial}{\partial |x|} - |p^0| \right) \Psi_{\text{scat}, \alpha} = 0$$

Mirror symmetry: $U(x_1, x_2) = U(x_1, -x_2)$ and the same for mass

Consequences:

$$\Psi_\alpha(x_1, x_2) = \Psi_{-\alpha}(x_1, -x_2)$$

$$\Psi_{\alpha, m}(x_1, x_2) = \sigma_x \Psi_{\alpha, -m}(x_1, -x_2)$$

If mass term is identically zero:

$$\Psi_\alpha(x_1, x_2) = \Psi_{-\alpha}(x_1, -x_2) = \sigma_x \Psi_{-\alpha}(x_1, x_2)$$

and therefore $\|\Psi_K(x_1, x_2)\| = \|\Psi_{K'}(x_1, x_2)\|$

Operators and symbols

$f(x, p)$ is a classical observable dependent on coordinates and momenta

It can be considered as a symbol of (pseudodifferential) operator $\text{Op}_t(f)$

$$\text{Op}_t(f)u(x) = \frac{1}{(2\pi\hbar)^n} \int e^{i\langle p, x-y \rangle / \hbar} f((1-t)x + ty, p) u(y) dy dp$$

Example:

$$f(x, p) = \langle x, p \rangle$$

$$\text{Op}_0(\langle x, p \rangle)u(x) = -i\hbar \langle x, \partial u(x) / \partial x \rangle$$

$$\text{Op}_0(\langle x, p \rangle) = \langle x, \hat{p} \rangle$$

but $\text{Op}_{1/2}(\langle x, p \rangle) = \frac{1}{2}(\langle x, \hat{p} \rangle + \langle \hat{p}, x \rangle)$

Operators and symbols II

$$f(x, p) = \sum_{\beta} f_{\beta}(x) p^{\beta}$$

$$p^{\beta} = \prod_i p_i^{\beta_i}$$

$$\text{Op}_0(f) = \sum_{\beta} f_{\beta}(x) \hat{p}^{\beta}$$

Oppositely, from operator to symbol: $a^{(t)} = \sigma_t(\hat{a})$ $\hat{a} = \text{Op}_t(a^{(t)})$

$$a^{(0)}(x, p, h) = \sigma_0(\hat{a}) = e^{-i\langle p, x \rangle / h} (\hat{a} e^{i\langle p, x \rangle / h})$$

$$a^{(t')} (x, p, h) = \exp \left(i h (t' - t) \left\langle \frac{\partial}{\partial x'}, \frac{\partial}{\partial p} \right\rangle \right) a^{(t)}(x, p, h)$$

Example:

$$\hat{a} = \frac{1}{2} (\langle x, \hat{p} \rangle + \langle \hat{p}, x \rangle)$$

$$a^{(0)} = \langle x, p \rangle - i \hbar / 2$$

$$a^{(1/2)} = \langle x, p \rangle$$

Operators and symbols III

Standard quantization: $t = 0$

$$\hat{a} u(x) = \text{Op}_0(a)u(x) = a(x, \hat{p}, \hbar)u(x) = \mathcal{F}_{p \rightarrow x}^{-1} a(x, p, \hbar) \mathcal{F}_{y \rightarrow p} u(y)$$

Weyl quantization: $t = 1/2$

$$\begin{aligned} \hat{a} u(x) &= \text{Op}_{1/2}(a)u(x) = a^W(x, \hat{p}, \hbar)u(x) \\ &= \frac{1}{(2\pi\hbar)^2} \int e^{i\langle p, x-y \rangle / \hbar} a\left(\frac{x+y}{2}, p, \hbar\right) u(y) dy dp \end{aligned}$$

Symbols are extremely convenient for expansion in \hbar

$$a^{(t)}(x, p, \hbar) = \sum_j a_j^{(t)}(x, p) \hbar^j$$

Operators and symbols IV

Symbol of adjoint operator: $\sigma_{1-t}(\hat{a}^\dagger) = [\sigma_t(\hat{a})]^\dagger$

Weyl symbol of self-adjoint operator is Hermitian matrix:

$$\sigma_{1/2}(\hat{a}) = \sigma_{1/2}(\hat{a}^\dagger) = [\sigma_{1/2}(\hat{a})]^\dagger$$

For Weyl symbols

$$\sigma(\hat{a}\hat{b}) = a(\mathbf{x}, \mathbf{p}, h)b(\mathbf{x}, \mathbf{p}, h) + \frac{ih}{2} \{a(\mathbf{x}, \mathbf{p}, h), b(\mathbf{x}, \mathbf{p}, h)\} + \mathcal{O}(h^2)$$

$$\{a, b\} = \left\langle \frac{\partial a}{\partial \mathbf{x}}, \frac{\partial b}{\partial \mathbf{p}} \right\rangle - \left\langle \frac{\partial a}{\partial \mathbf{p}}, \frac{\partial b}{\partial \mathbf{x}} \right\rangle$$

Poisson bracket

Commutators and Poisson brackets

$$\sigma_{1/2}([\hat{a}, \hat{b}]) = ih\{a^W, b^W\} + \mathcal{O}(h^3)$$

Semiclassics for matrix Hamiltonians

Belov *et al.*, J Eng Math 55, 183 (2006); Littlejohn, Flynn, Phys Rev A 44, 5239 (1991)

$\hat{H}\Psi = E\Psi$, where \hat{H} is an $n \times n$ matrix

Ψ is an n -dimensional vector

We try the solution

$$\Psi(\mathbf{x}) = \hat{\chi} \psi(\mathbf{x})$$

ψ is an effective scalar wavefunction

$$\hat{L}\psi = E\psi$$

\hat{L} plays the role of the scalar Hamiltonian

Operator equation to solve

$$\hat{H}\hat{\chi} - \hat{\chi}\hat{L} = 0$$

Matrix Hamiltonians II

In zeroth order in \hbar

$$H_0(\mathbf{x}, \mathbf{p})\chi_0(\mathbf{x}, \mathbf{p}) = L_0(\mathbf{x}, \mathbf{p})\chi_0(\mathbf{x}, \mathbf{p})$$

which means that the principal symbols L_0 and χ_0 are the eigenvalues and eigenvectors, respectively, of the principal symbol of the matrix Hamiltonian \hat{H} .

Note that H_0 is an $n \times n$ matrix and χ_0 is an n -dimensional vector.

First order in \hbar

$$L_1 = \underbrace{-i\chi_0^\dagger \{\chi_0, L_0\}}_{\text{Berry part } L_{1B}} - \underbrace{\frac{i}{2} \sum_{j,k} (H_{jk} - L_0 \delta_{jk}) \{\chi_{0,j}^*, \chi_{0,k}\}}_{\text{Additional part } L_{1A}}$$

2D Dirac Hamiltonian

$$L_0^\pm(\mathbf{x}, \mathbf{p}) = U(\mathbf{x}) \pm \sqrt{p^2 + m^2(\mathbf{x})}$$

$$L_{1,\alpha}^\pm(\mathbf{x}, \mathbf{p}) = \frac{\alpha}{2\sqrt{p^2 + m^2}(\sqrt{p^2 + m^2} \mp m)} \left(p_2 \frac{\partial(U+m)}{\partial x_1} - p_1 \frac{\partial(U+m)}{\partial x_2} \right)$$

Semiclassical solution

Semiclassical Ansatz $\psi(\mathbf{x}) = \varphi(\mathbf{x})e^{iS(\mathbf{x})/\hbar}$, $\varphi = \varphi_0 + \hbar\varphi_1 + \dots$
to solve the scalar (pseudodifferential) equation $\hat{L}\psi = E\psi$

Terms of order

\hbar^0 Hamilton-Jacobi equation $L_0(\mathbf{x}, \partial S/\partial \mathbf{x}) = E$: trajectories

\hbar^1 Transport equation: determines φ_0

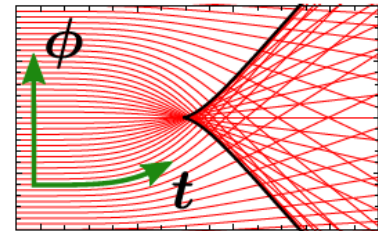
Final solution

$$\psi(\mathbf{x}) = \frac{\exp(i\Phi_{sc}(\mathbf{x}))}{\sqrt{J(\mathbf{x})}} \exp(iS(\mathbf{x})/\hbar)$$

$$\Phi_{sc}(\mathbf{x}) = \int_0^t L_1(\mathbf{X}(t, \phi), \mathbf{P}(t, \phi)) dt$$

$$J(\mathbf{x}) = \det(\mathbf{X}_t, \mathbf{X}_\phi), \quad S(\mathbf{x}) = \int_0^x \langle \mathbf{P}, d\mathbf{X} \rangle$$

Solution to the original eigenvalue equation $\Psi(\mathbf{x}) = \hat{\chi}\psi(\mathbf{x})$



ϕ labels initial conditions

Semiclassical solution II

Hamilton-Jacobi equations are equivalent to Hamilton's equations

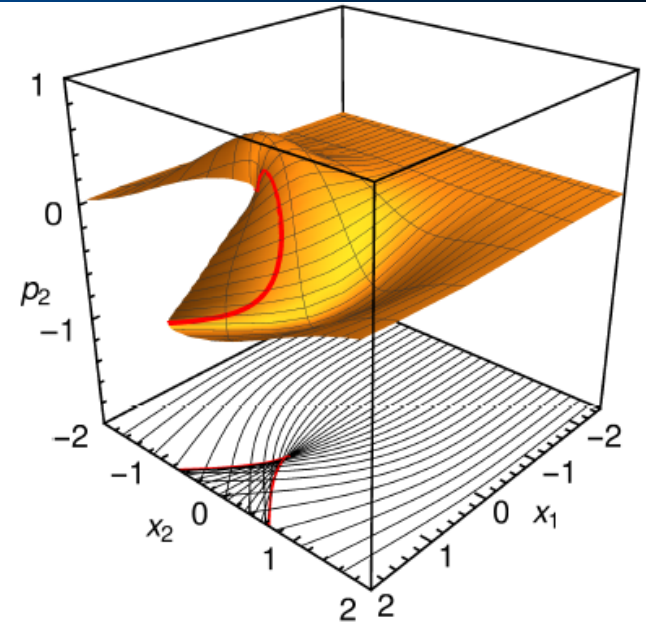
Lift the trajectories to phase space

Jacobian $J = \det(\mathbf{X}_t, \mathbf{X}_\phi) \neq 0$ when this surface can be projected onto \mathbf{X}

Caustic: $J = 0$, density of trajectories infinite

Asymptotic solution $\psi(\mathbf{x}) = \frac{\exp(i\Phi_{sc}(\mathbf{x}))}{\sqrt{J(\mathbf{x})}} \exp(iS(\mathbf{x})/h)$

diverges at caustic: focusing occurs



Further: Lagrange manifolds, canonical operator, eikonal coordinates etc.

Caustics and semiclassics

$$\tilde{U}(\tilde{x}) = -\tilde{U}_0 \exp(-\tilde{x}^2)$$

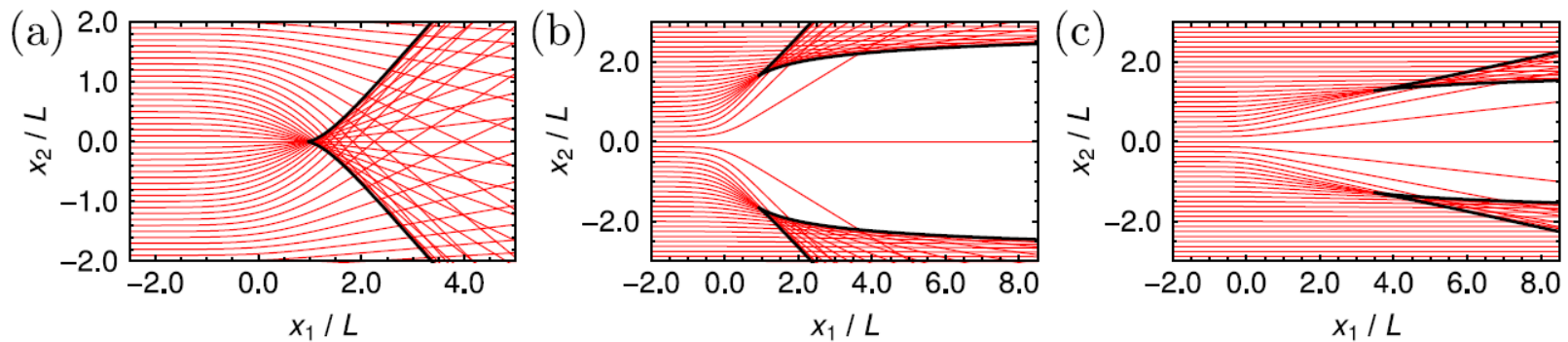


Fig. 3. Trajectories obtained by integrating Hamilton's equations (77) for different potentials $\tilde{U}(\tilde{x})$ and masses $\tilde{m}(\tilde{x})$. The black lines indicate the caustics. (a) Gaussian potential well (171) with $\tilde{U}_0 = \frac{1}{2}$ and $\tilde{m}(\tilde{x}) = 0$. (b) Gaussian potential barrier (171) with $\tilde{U}_0 = -\frac{1}{2}$ and $\tilde{m}(\tilde{x}) = 0$. (c) Gaussian mass $\tilde{m}(\tilde{x}) = \tilde{m}_0 \exp(-\tilde{x}^2)$ with $|\tilde{m}_0| = \frac{1}{2}$ and $\tilde{U}(\tilde{x}) = 0$.

Caustics and semiclassics II

For $m = 0$:

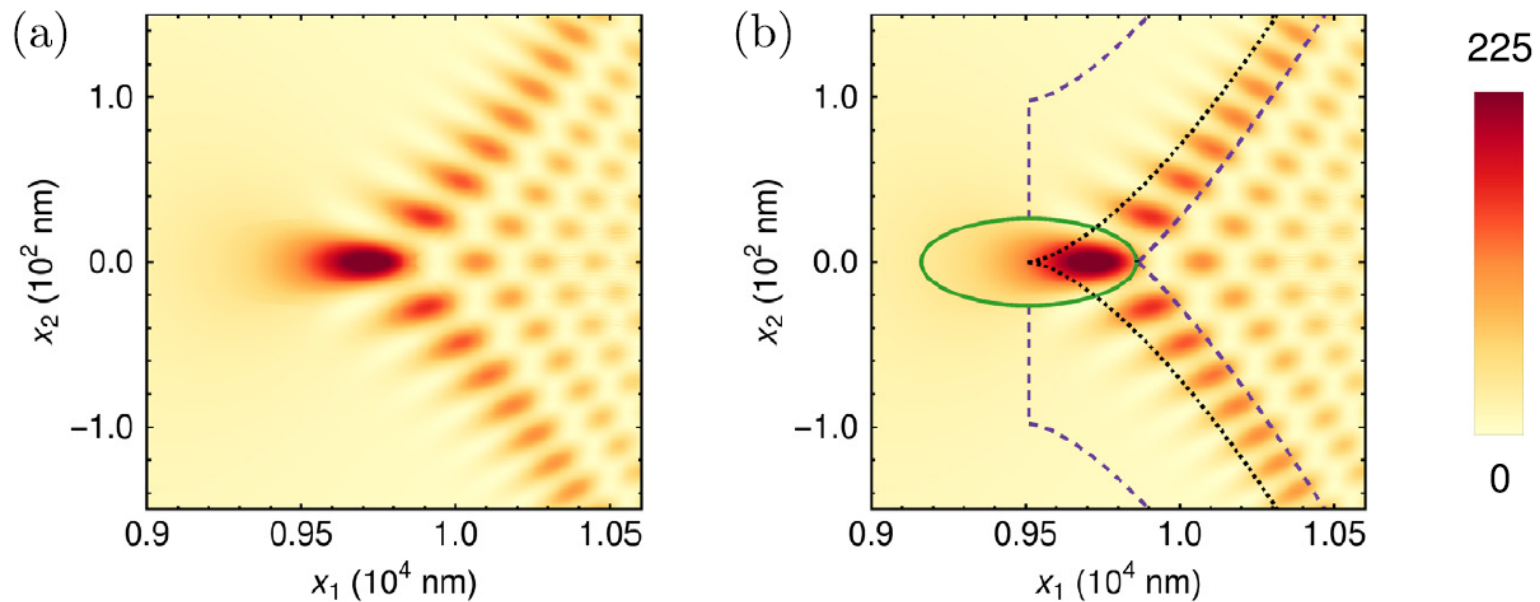


Fig. 5. (a) Intensity $\|\Psi\|^2 = \Psi^\dagger \Psi$ obtained by using the various semiclassical approximations in the appropriate regions. (b) The intensity $\|\Psi\|^2$ together with the regions in which the various approximations were used. The Pearcey approximation (156) was used inside the green ellipse, while the Airy approximation (153) was used between the dashed purple lines. The WKB approximation (145) was used to create the rest of the figure. The dotted black line represents the caustic.

Semiclassical equations of motion

$$\frac{dx_j}{dt} = \frac{\partial L_0}{\partial p_j} + \hbar \frac{\partial L_{1,A}^W}{\partial p_j} + \hbar \sum_k (\Omega_{pp})_{jk} \frac{\partial L_0}{\partial x_k} - \hbar \sum_k (\Omega_{px})_{jk} \frac{\partial L_0}{\partial p_k},$$
$$\frac{dp_j}{dt} = -\frac{\partial L_0}{\partial x_j} - \hbar \frac{\partial L_{1,A}^W}{\partial x_j} - \hbar \sum_k (\Omega_{xp})_{jk} \frac{\partial L_0}{\partial x_k} + \hbar \sum_k (\Omega_{xx})_{jk} \frac{\partial L_0}{\partial p_k}.$$

$$(\Omega_{xp})_{jk} = i \left(\frac{\partial \chi_0^\dagger}{\partial x_j} \frac{\partial \chi_0}{\partial p_k} - \frac{\partial \chi_0^\dagger}{\partial p_k} \frac{\partial \chi_0}{\partial x_j} \right)$$

is the Berry curvature (This derivation: Littlejohn & Flynn 1991)

As used in the theory of topological matter

Xiao, Chang & Niu, RMP 82, 1959 (2010)

The role of semiclassical phase

$$L_0(x, p) = \sqrt{p^2 + m^2(x)} + U(x) = E$$

Can be rewritten as

$$\mathcal{L}_0(x, p) \equiv C(x)|p| = 1, \quad \text{where } C(x) = \frac{1}{\sqrt{(E - U(x))^2 - m^2(x)}}$$

(a new “Hamiltonian”, new “energy” = 1)

When we set

$$U(x) = E - \sqrt{E^2 - m^2(x)}$$

$$C(x) = \frac{1}{\sqrt{(U(x) - E)^2 - m^2(x)}} = \frac{1}{E}$$

and classically there is no effect on electron motion.

Only semiclassical phase matters in this situation

The role of semiclassical phase II

$$\tilde{m}(\tilde{x}) = \frac{3}{8} \left(1 - \frac{1}{\cosh \left[\frac{5}{4} \tilde{x}_2 \right]} \right) \left(\tanh \left[\frac{9}{5} (\tilde{x}_1 - \tilde{x}_{1,b1}) \right] - \tanh \left[\frac{9}{5} (\tilde{x}_1 - \tilde{x}_{1,b2}) \right] \right)$$

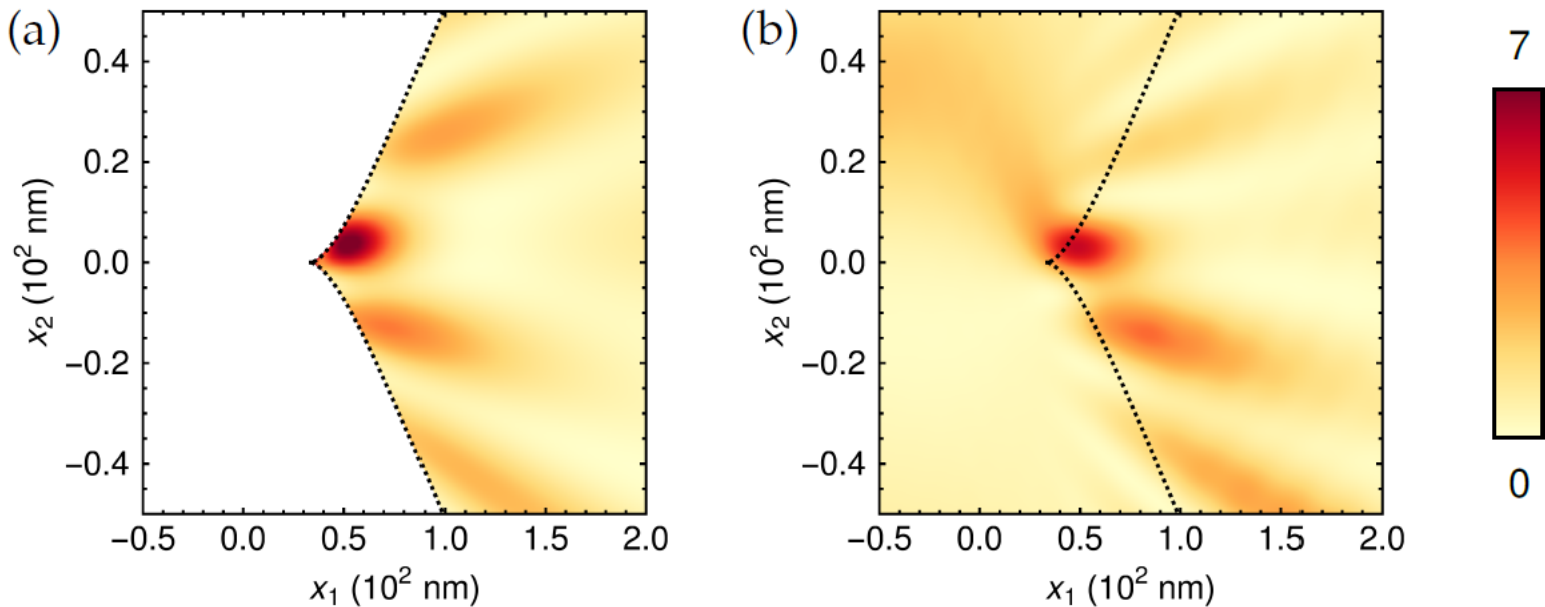


Figure 6.8: Comparison of the intensity $\|\Psi_{K'}\|^2$ for electrons in the K' -valley with $E = 200$ meV. The incoming electrons are focused by the Gaussian potential (6.23) with $U_0 = 100$ meV and $L = 35.5$ nm. In front of this potential, there is a region in which the mass is given by equation (6.26) with $\tilde{x}_{1,b1} = -10$ and $\tilde{x}_{1,b2} = -5$ and the potential is given by equation (6.24). (a) Result of the uniform approximation (b) Result of a tight-binding calculation for a zigzag sample with a width of $4000 a_{CC} \approx 568$ nm.

The role of semiclassical phase III

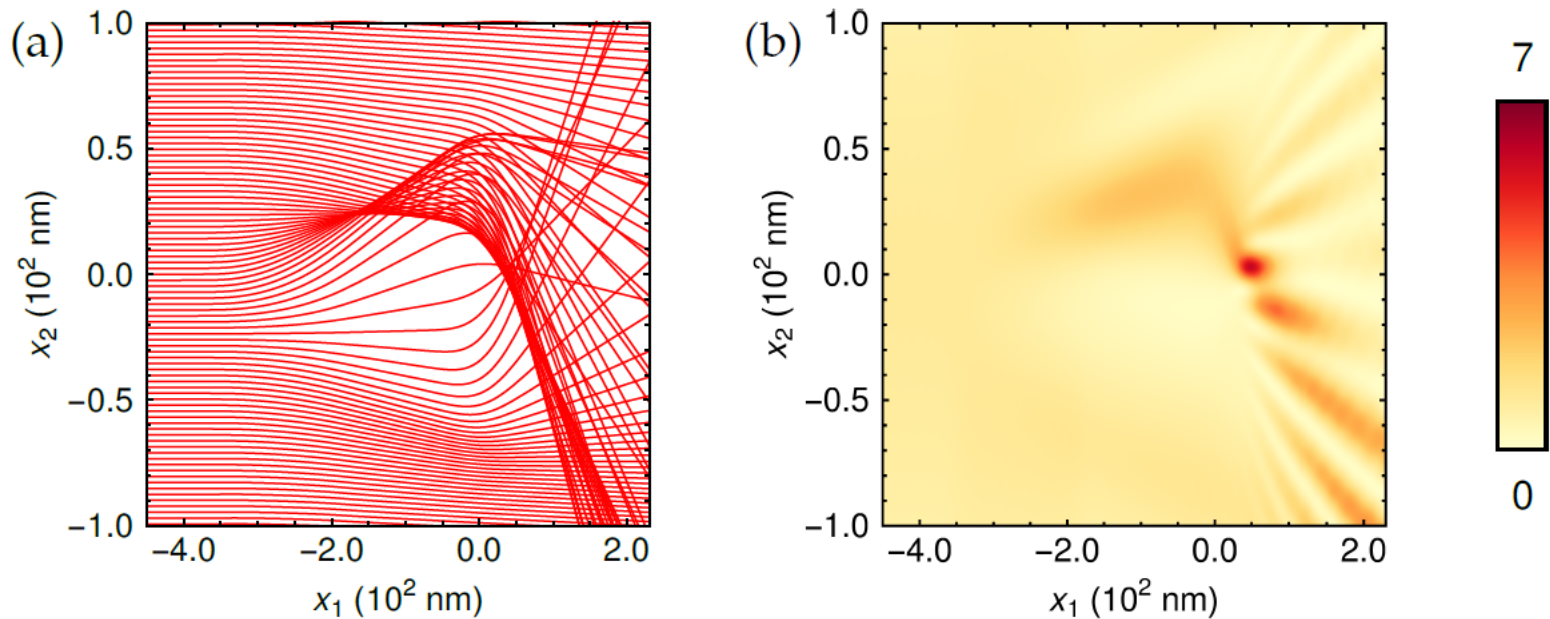


Figure 6.9: (a) Trajectories for an electron in the K' valley, computed using the modified equations of motion (6.27). (b) Result of a tight-binding calculation for a zigzag sample with a width of $4000 a_{CC} \approx 568$ nm. To produce these figures, we used the same parameters as in figure 6.8.

Conclusions

Semiclassical approximation is not only a qualitative tool to understand numerical data (which is very important by itself) but also frequently gives you quite accurate quantitative results

Still open questions:

- Tunneling in more than one dimension;
- Tunneling in bilayer graphene;
- Further issues on zero-mass lines, spectral flow etc.